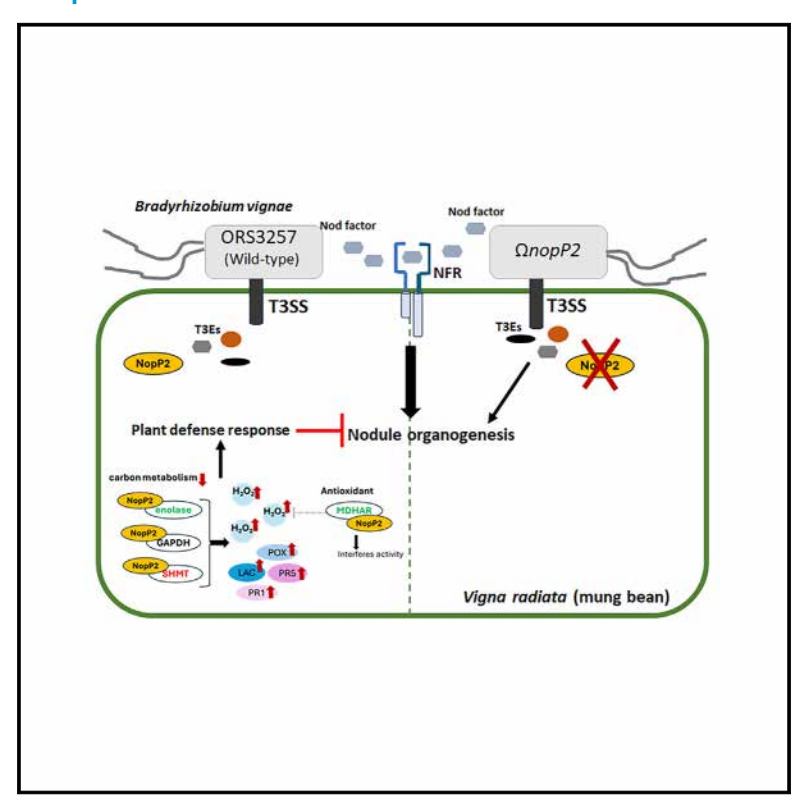
iScience

Elucidation of the symbiotic incompatibility mechanisms between *Vigna radiata* and *Bradyrhizobium vignae* ORS3257 mediated by nodulation outer protein P2

Graphical abstract



Authors

Pongpan Songwattana, Pakpoom Boonchuen, Natcha Pruksametanan, ..., Nantakorn Boonkerd, Panlada Tittabutr, Neung Teaumroong

Correspondence

panlada@sut.ac.th (P.T.), neung@sut.ac.th (N.T.)

In brief

Interaction of plants with organisms; Plant Biology; Plant pathology

Highlights

- B. vignae NopP2 triggers V. radiata defense
- NopP2 binds enolase, GAPDH, MDHAR, SHMT; disrupts redox
- NopP2-induced H₂O₂ drives *V. radiata* symbiosis incompatibility





iScience



Article

Elucidation of the symbiotic incompatibility mechanisms between *Vigna radiata* and *Bradyrhizobium vignae* ORS3257 mediated by nodulation outer protein P2

Pongpan Songwattana,^{1,8} Pakpoom Boonchuen,^{2,8} Natcha Pruksametanan,² Kamonluck Teamtisong,³ Shusei Sato,⁴ Shun Hashimoto,⁴ Nahoko Higashitani,⁴ Yasuyuki Kawaharada,⁵ Masato Araragi,⁵ Shin Okazaki,⁶ Pongdet Piromyou,¹ Jenjira Wongdee,¹ Teerana Greetatorn,¹ Eric Giraud,⁷ Nantakorn Boonkerd,² Panlada Tittabutr,^{2,*} and Neung Teaumroong^{2,9,*}

SUMMARY

Bradyrhizobium vignae ORS3257 is an efficient symbiotic strain for Vigna unguiculata and V. mungo but fails with V. radiata due to an effector-triggered immunity response mediated by the nodulation outer protein P2 (NopP2). To understand this incompatibility, we identified NopP2 interacting proteins in V. radiata cv. KPS1, including enolase, glyceraldehyde-3-phosphate dehydrogenase (GAPDH), monodehydroascorbate reductase (MDHAR), and serine hydroxymethyltransferase (SHMT) as targets. Protein-protein interaction assays confirmed that NopP2 binds to these enzymes, and further analysis revealed their co-localization on the plasma membrane. Comparative transcriptomic analysis revealed NopP2 stimulates genes related to plant defense response (PR1, PR5, MYB13, and TAO1), hydrogen peroxide (SOD, POX10, and POX16), and cell wall lignification (LAC). NopP2 did not alter the expression of genes encoding the target enzymes but interfered with MDHAR activity, leading to high H₂O₂ accumulation in roots. These findings suggest that NopP2 contributes to symbiotic incompatibility in V. radiata by inducing a multifaceted defense response and initiating cell wall lignification early in infection.

INTRODUCTION

Legume-rhizobium symbiosis is a key process in returning atmospheric nitrogen (N_2) to the environment via a nitrogen fixation reaction. This symbiotic relationship allows legumes to form root nodules for rhizobia, which convert N_2 into ammonia (N_3) for use in the plant. In return, the plant offers a conducive environment for nitrogen fixation and provides carbon sources for bacterial growth. Nodule formation depends on complex regulations and mutual signal exchanges between hosts and symbionts. The plant secretes flavonoid compounds that are recognized by the rhizobia, inducing the production of Nod factors (N_3). These N_3 are then perceived by the plant, triggering cortical cell division to form nodule primordia and initiating the infection process.

In some cases, successful symbiosis requires the cooperation of NFs signaling and the Type III Secretion System ${\sf System}$

(T3SS). Some rhizobia use T3SS to deliver effector proteins (T3Es) directly into host cells, overcoming plant immunity and promoting infection.^{2–4} In some cases, rhizobial T3Es act similarly to pathogenic T3Es, where specific recognition by plant resistance proteins (R) can trigger an effector-triggered immunity (ETI) response, often resulting in plant cell death and symbiosis abortion.^{5,6} However, the specific protein-protein interactions between rhizobial T3Es and plant proteins remain largely unknown.

Mutation analysis of T3Es provides important information about their roles in host-specific interaction. For example, the mutation of *nopT* and *nopAB* in *B. vignae* ORS3257 has drastically affected the ability of ORS3257 to develop an efficient symbiosis with *V. unguiculata* and *V. mungo.* Similarly, the mutation of *nopM* (encoding E3 ubiquitin ligase) in *Sinorhizobium* sp. NGR234 revealed a positive role in the symbiotic initiation with *Lablab purpureus.* Conversely, *nopE* mutation in



¹Institute of Research and Development, Suranaree University of Technology, Nakhon Ratchasima 30000, Thailand

²School of Biotechnology, Institute of Agricultural Technology, Suranaree University of Technology, Nakhon Ratchasima 30000, Thailand

³The Center for Scientific and Technological Equipment, Suranaree University of Technology, Nakhon Ratchasima 30000, Thailand

⁴Graduate School of Life Sciences, Tohoku University, Sendai 980-8577, Japan

⁵Department of Plant Bio Sciences, Faculty of Agriculture Iwate University, 3-18-8 Ueda, Morioka, Iwate 202-8133, Japan

⁶Institute of Agriculture, Tokyo University of Agriculture and Technology, Fuchu, Tokyo 183-8538, Japan

⁷IRD/CIRAD/INRAE, PHIM, Plant Health Institute of Montpellier, UMR-PHIM, Université de Montpellier/Institut Agro, 34398 Montpellier, France

⁸These authors contributed equally

⁹Lead contact

^{*}Correspondence: panlada@sut.ac.th (P.T.), neung@sut.ac.th (N.T.) https://doi.org/10.1016/j.isci.2025.112351



B. diazoefficiens USDDA110 enhances the nodulation efficiency with *V. radiata* cv. KPS2, but it reduced nodulation efficiency with *V. radiata* cv. CN72 and KPS1. Therefore, T3Es secreted by the T3SS of rhizobia can either promote or inhibit nodulation, depending on the host plant species. ¹⁰

B. vignae ORS3257 is recognized for its efficiency in forming symbiotic relationships with *V. unguiculata* and *V. mungo*. However, this strain is unable to form nodules on *V. radiata* (mung bean).⁷ A total of 27 putative effector proteins were identified in the ORS3257 genome, including two *nopP* homologs, *nopP1* and *nopP2*, located in different regions of the symbiotic island. It has been shown that the specific mutation in *nopP2* restores functional symbiosis between ORS3257 and *V. radiata*, indicating that NopP2 is responsible for this incompatibility.⁷

NopP protein has been reported as a key regulator for rhizobial infection and nodule organogenesis in other legumes. NopP in *Sinorhizobium* sp. strain NGR234 was shown to be a major determinant of nodulation *in Flemingia congesta* and *Tephrosia vogelii*. ^{11,12} NopP in *B. elkanii* USDA122 negatively regulates nodulation with Rj2-soybeans via ETI. ¹³ Conversely, the mutation of *nopP* in *Mesorhizobium huakuii* leads to decreased nodule formation in *Astragalus sinicus*. ¹⁴ This is similar to the Nopl effector of *S. fredii* HH103, which is currently annotated as *nopP* (GenBank: CCE98653.1). Inactivation of this *nopP* gene reduces both the number of nodules and the dry mass of nodules formed by *Glycine max* cv. Williams 82, *V. unguiculata* (cowpea), and *Lotus burttii*, indicating the positive role of NopP in symbiosis in these cases. ^{15,16}

Although NopP has recently been identified in various rhizobial strains to be key T3Es modulating their symbiotic properties, its biological functions and targets remain poorly understood, which, in addition, could also be different from one symbiotic model to another. It has recently been reported that NopP from B. diazoefficiens USDA110 directly interacts with GmNNL1 (G. max Nodule Number Locus 1) and inhibits G. max nodulation by triggering the plant ETI.¹⁷ NopP from M. amorphae specifically interacts with TRAPPC13 (Trafficking protein particle complex subunit 13-like), which plays a role during the early infection process. 18 Moreover, a G-type receptor-like kinase (AsNIP43) has recently been identified as the target of NopP from M. huakuii, which negatively regulates the symbiosis nodulation on Chinese milk vetch (A. sinicus). 14 However, the molecular mechanism through which host legume plants sense NopP remains largely unknown. In addition, the target(s) of NopP from the B. vignae strain ORS3257 during V. radiata interaction have not been identified.

In this study, we characterized multiple NopP2-interacting proteins using an *in vitro* pull-down assay. The protein-protein interaction analysis, confirmed by additional *in vivo* and subcellular localization in *planta*, identified enolase, glyceraldehyde-3-phosphate dehydrogenase (GAPDH), monodehydroascorbate reductase (MDHAR), and serine hydroxymethyltransferase (SHMT) as NopP2-interacting partners. Moreover, plant response mechanisms via NopP2 function revealed that NopP2 induces a multifaceted plant defense response, especially H₂O₂ accumulation, leading to incompatible *V. radiata* symbiosis.

RESULTS

Nodulation outer protein P2 mediates symbiotic incompatibility in *Vigna radiata* cultivars through *B. vignae* ORS3257 and complemented strain SUTN9-2

To confirm the negative effect of NopP2 of ORS3257 during interaction with various V. radiata cultivars, 12 mung bean (or various) cultivars from different countries (listed in Table S1) were inoculated with ORS3257 and its derivative mutants (Δ T3SS and Ω nopP2). Mutation of structural T3SS (Δ T3SS) and NopP2 (Ω nopP2) leads to enhanced plant growth and nodule formation in V. radiata cv. KPS1 and KPS2 (Figures 1A–1J). Interestingly, nodulation phenotypes in all mung bean tests showed consistent results: nodulation by the WT strain ORS3257 was completely abolished, while the Δ T3SS and Ω nopP2 mutants induced high numbers of effective nodules (Table S1). These results indicate that NopP2 plays a general negative role during the interaction of ORS3257 and all the V. radiata (mung bean) cultivars tested.

To confirm that the phenotype observed for Δ T3SS and Ω nopP2 mutants was indeed related to the absence of the secretion of NopP2. Therefore, we compared the secretomes of the WT strain and its derivative mutants (Δ T3SS and Ω nopP2) under genistein induction. The result confirmed that NopP2 was secreted in a T3SS-dependent manner. The NopP2 protein band was not detected in the secretome of the Δ T3SS and Ω nopP2 mutants, while it was present in the secretome of the ORS3257 (WT) strain (Figure 2A). These findings indicated that the symbiotic incompatibility phenotypes observed in the Δ T3SS and Ω nopP2 mutants were attributable to the absence of NopP2 in ORS3257.

The next question is: Does the function of NopP2 confer symbiotic incompatibility with other Bradyrhizobium strains? To investigate this, Bradyrhizobium sp. SUTN9-2, an effective mung bean symbiont possessing a T3SS, was transformed with replicative plasmid pMG103-nptII-cefor containing 6×His-tagged NopP2 from ORS3257. This complemented strain, designated 9-2+nopP2, carries the T3SS and expresses the heterologous NopP2 protein. Analysis of the proteins secreted in the supernatant showed that the NopP2-6×His protein was successfully secreted by the complemented strain 9-2+nopP2 under genistein induction (+Gen) (Figure 2B), albeit at a low level. Furthermore, the symbiotic properties of the complemented strain 9-2+nopP2 were strongly negatively impacted it as observed a reduced nodule size and number, lower nitrogenase activity, and reduced overall plant growth of V. radiata cv. KPS1 in comparison with the wild-type SUTN9-2 (Figures 2C-2E). These findings suggest that NopP2 from ORS3257 consistently exerts a negative effect on mung bean symbiosis, but it exerts a minor effect on nodulation efficiency when SUTN9-2 secretes NopP2.

To test the hypothesis that NopP2 of ORS3257 disrupts symbiosis when produced within plant roots, we generated transgenic mung bean roots expressing *nopP2-GFP* fusion under the control of the strong CaMV35S promoter. *Agrobacterium rhizogenes* strain K599 was used to transform *V. radiata* and generate hairy roots. Root expression of NopP2-GFP and control constructs expressing only GFP (35S:GFP) was confirmed using green fluorescence microscopy. Transgenic and non-transgenic



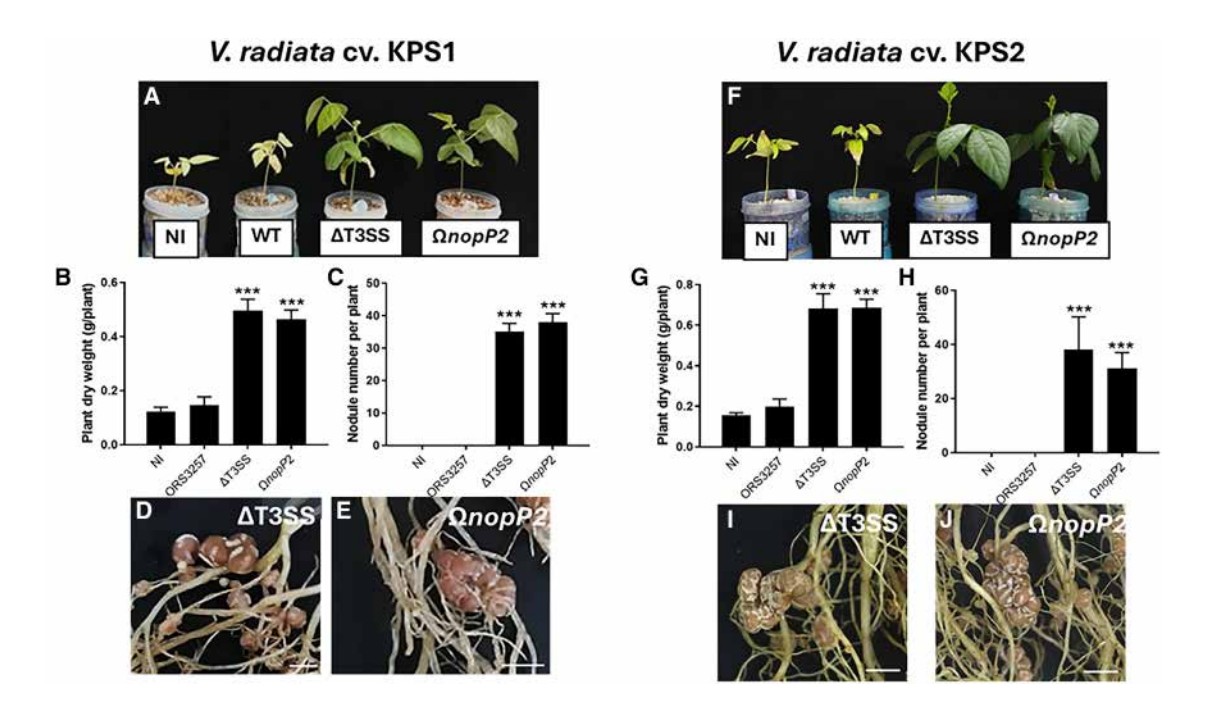


Figure 1. Nodulation phenotypes of *Bradyrhizobium vignae* ORS3257 and its derivative T3SS (Δ T3SS) and nopP2 (Ω nopP2) mutants were evaluated in different cultivars of *Vigna radiata*

In *V. radiata* cv. KPS1 (A–E) and KPS2 (F–J), plant phenotypes (A and F), dry weights (B and G), and nodule number (C and H) were compared between plants inoculated with ORS3257, Δ T3SS, Ω nopP2, and non-inoculated (NI) controls. Data are means \pm SD (n = 5). Asterisks indicate significant differences compared to WT (***p < 0.001). The nodule morphologies (D, E, I, and J) were compared between plants inoculated with Δ T3SS and Ω nopP2. Scale bars = 2 mm.

roots were obtained from the same plant (transgenic roots indicated by white arrows in Figures 2G–2N). The transgenic roots were confirmed by PCR using specific primers for the 35S promoter and Nos-terminator. The target sizes of 35S:GFP (1,614-bp) and 35S:NopP2-GFP (2,454-bp) were detected at their corresponding sizes, whereas non-transgenic roots were not detected (Figure 2F). The transgenic roots (35S:GFP and 35S:nopP2-GFP) were subsequently inoculated with ORS3257 wild-type and Ω nopP2 mutant strains to evaluate the nodulation phenotypes. It is noted that the Ω nopP2 mutant was previously constructed by single homologous recombination with the pVO155-npt2-cefo-npt2-GFP plasmid, allowing the nodules derived from this strain to exhibit green fluorescence due to a constitutive expression of the GFP.

As expected, transgenic roots expressing NopP2-GFP, such as 35S:GFP control and non-transgenic roots, failed to form nodules when inoculated with ORS3257 (Figures 2G, 2H, 2K, and 2L). Conversely, while 35S:GFP and non-transgenic roots successfully formed symbiotic nodules with Ω nopP2. Remarkably, NopP2-GFP transgenic mung bean roots were able to block nodulation induced by the nodulating strain Ω nopP2 (Figures 2I–2N). These findings suggest that NopP2 overexpression significantly inhibits symbiotic nodulation, even in the absence of the native nopP2 gene in the bacterial strain.

Multiple interacting proteins identified as targets of nodulation outer protein P2

To identify the target proteins of NopP2, an in vitro pull-down assay was conducted to detect physical interactions between

NopP2 and proteins from mung bean roots. Recombinant NopP2 tagged with 6×His was overproduced by the E. coli pET system. The purified NopP2-His was used as bait to capture its targets from total root proteins of plants with and without ORS3257 inoculation (Figures 3A and 3B). The incubation of NopP2-His with total root proteins revealed five significant bands that were not observed in a single incubation (only root proteins or NopP2-His) (Figure 3C). These five bands were selected for MS/MS analysis. Five proteins with the top matches in the database were identified as candidate interacting proteins for NopP2: enolase, glyceraldehyde-3-phosphate dehydrogenase (GAPDH), monodehydroascorbate reductase (MDHAR), Aspartate aminotransferase (AST), and serine hydroxymethyltransferase (SHMT) (Figure 3D). All proteins were identified from the incubation of NopP2-His and protein extracts from non-inoculated roots, while enolase and GAPDH were also detected in NopP2-His incubated with ORS3257-inoculated roots.

To confirm their interaction, an *in vitro* pull-down assay and ELISA were performed using individually purified proteins. The full-length proteins of each candidate were overexpressed in the pET system to obtain purified 6×His-tagged proteins, whereas NopP2 was tagged with GST. The purified proteins were detected using SDS-PAGE and confirmed by Western blot analysis (Figures S1A–S1G). The purified GST protein was used as a control for the ELISA (Figure S1B). The results of the pull-down assay demonstrated that NopP2-GST immobilized in the column directly bound to Enolase-His, GAPDH-His, MDHAR-His, and SHMT-His. Western blot analysis successfully detected both the interacting proteins and NopP2



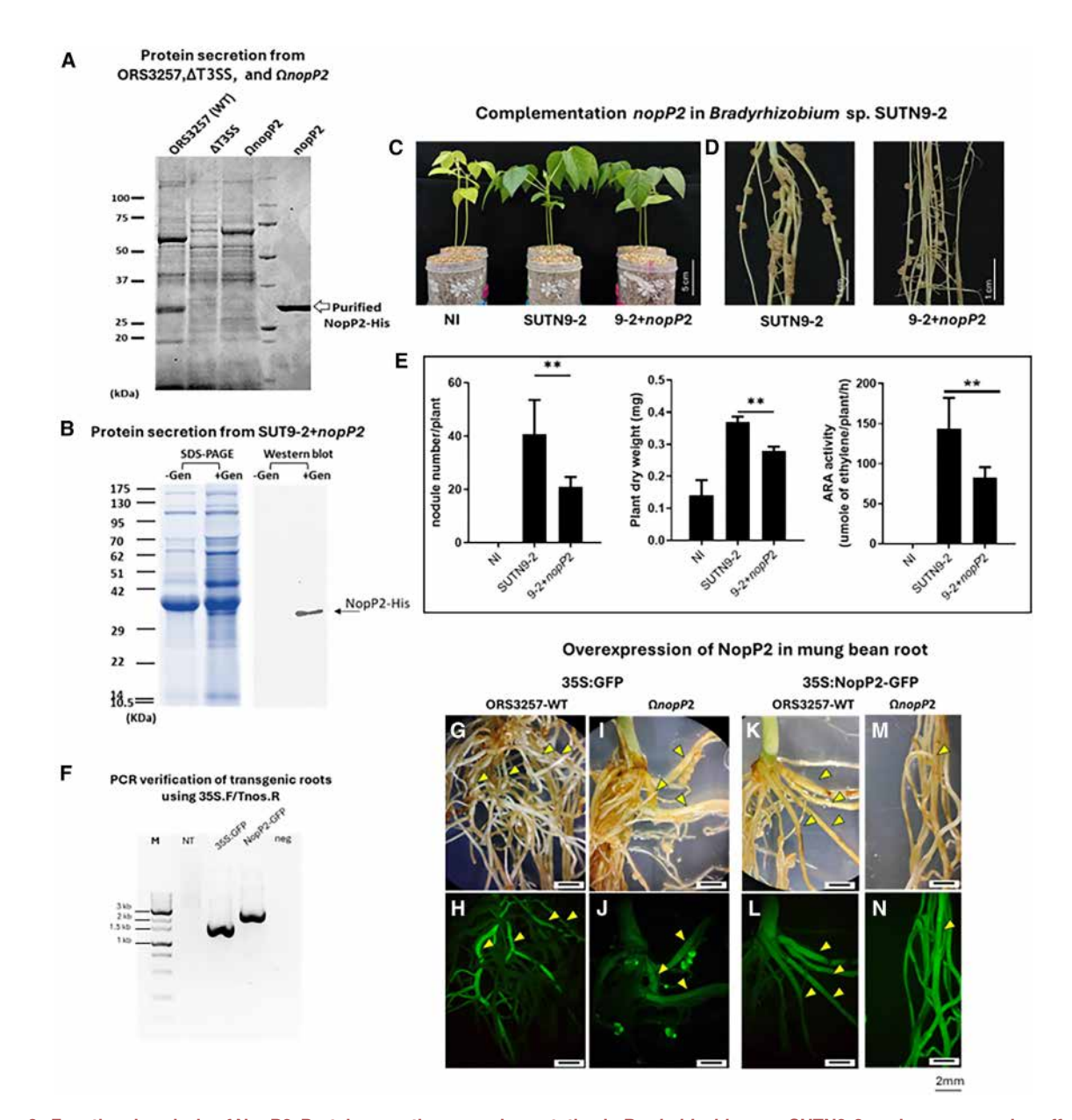


Figure 2. Functional analysis of NopP2: Protein secretion, complementation in *Bradyrhizobium* sp. SUTN9-2, and overexpression effects in mung bean roots

(A) Protein secretion profiles of *B. vignae* ORS3257, T3SS (Δ T3SS) and *nopP2* mutants (Ω nopP2) cultured in AG medium with (+Gen) induction. Purified NopP2-His (pNopP2) was used as a positive control for the NopP2-His band target (indicated by an arrow).

(B) Secretion proteins from Bradyrhizobium sp. SUTN9-2 complemented with nopP2 (annotated as 9-2+nopP2) were determined by SDS-PAGE and Western blot with anti-His antibodies, with protein secretions extracted from cell-free cultures with (+Gen) and without genistein (-Gen) induction.

(C–E) Nodulation phenotypes in *V. radiata* cv. KPS1 nodulated by SUTN9-2 wild type and 9-2+nopP2 compared with non-inoculated (NI) plants at 21 dpi: plant phenotypes (C), nodule phenotypes (D), and nodulation efficiency presented by nodule numbers, plant dry weight, and ARA activity (E). Data are means \pm SD (n = 5). Asterisks indicate significant differences compared to WT (**p < 0.01).

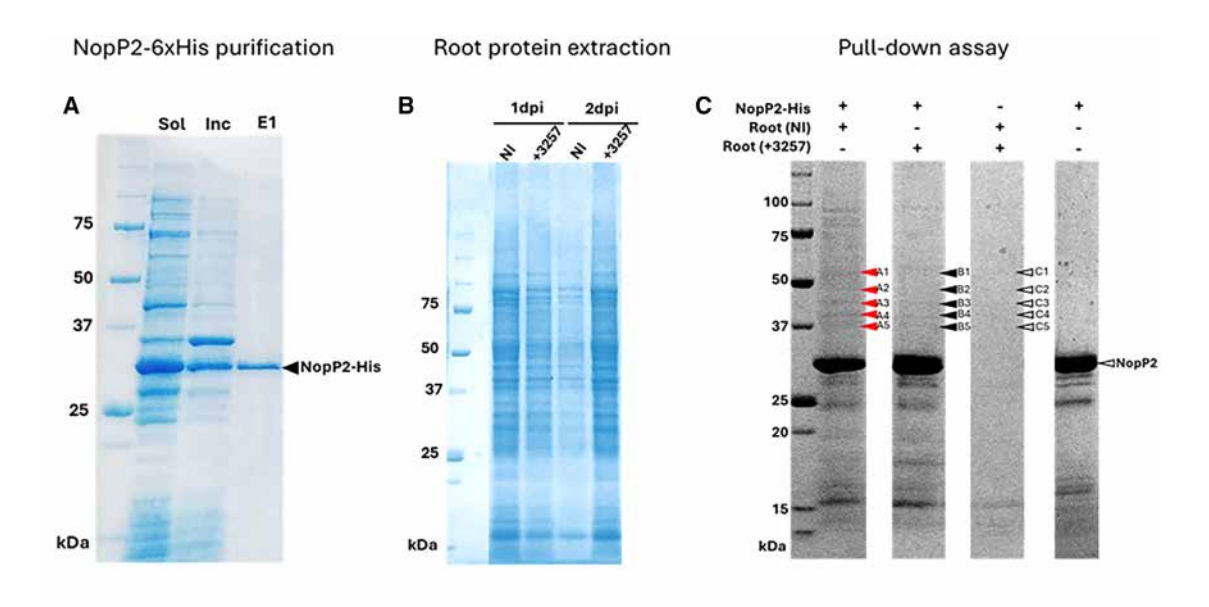
(F) PCR verification of total gDNA extracted from non-transgenic roots (NT), transgenic roots expressing GFP (35S:GFP), and transgenic roots expressing NopP2-GFP (35S:NopP2-GFP). Target bands were amplified using specific primers on the CaMV35S promotor and Nos-terminator, showing the corresponding sizes for 35S:GFP (1,614-bp) and 35S:NopP2-GFP (2,454-bp).

(G-N) Root and nodule phenotypes of 35S:GFP and 35S:NopP2-GFP after inoculation with ORS3257 and Ω nopP2. Roots images under brightfield and fluorescence microscopy were compared. Transgenic roots with green fluorescence are indicated by yellow head arrows.

(Figures 4A-4D). In contrast to AST-His, only NopP2-GST was retained in the column during the incubation with AST-His (Figure S1G).

These results indicate that Enolase, GAPDH, MDHAR, and SHMT are the interacting partners of NopP2, while AST does not interact. Moreover, the specific protein-protein interactions





D MS-Fit search results of protein bands display top matches in database

Protein Band	Gene	Sequence coverage (%)	pl	Molecular weight (kDa)		NCBI accession no.
				Observed	Theory	. accession no.
A1	Serine hydroxymethyltransferase (SHMT)	23.1%	6.8	52	51.786	XP_014521732.1
A2, B2	Enolase	20.5%	5.5	48	47.734	XP_014496230.1
А3	Monodehydroascorbate reductase (MDHAR)	20.1%	5.6	45	46.809	XP_014514196.1
A4	Aspartate aminotransferase (AST)	17.8%	7.7	43	49.674	XP_014499632.1
A5, B5	Glyceraldehyde-3-phosphate dehydrogenase (GAPDH)	25.0%	7.0	37	36.901	XP_014494377.1

Figure 3. SDS-PAGE and MS/MS analysis results from in vitro pull-down assay

(A) SDS-PAGE of NopP2-6×His purification performed by using a Ni-column. Proteins from soluble (Sol) and inclusion bodies (Inc), and purified NopP2-His were determined.

- (B) SDS-PAGE of total root proteins from V. radiata cv. KPS1 roots with and without inoculation with ORS3257.
- (C) SDS-PAGE from in vitro pull-down assay.
- (D) MS-fit search results of protein bands display top matches in the database (NCBI RefSeq: GCF_000741045.1).

of these four proteins with NopP2 were further confirmed by ELISA, suggesting relatively strong associations (Figures 4E-4H). Therefore, the results from both assays indicate that Enolase, GAPDH, SHMT, and MDHAR can directly bind to NopP2 from ORS3257.

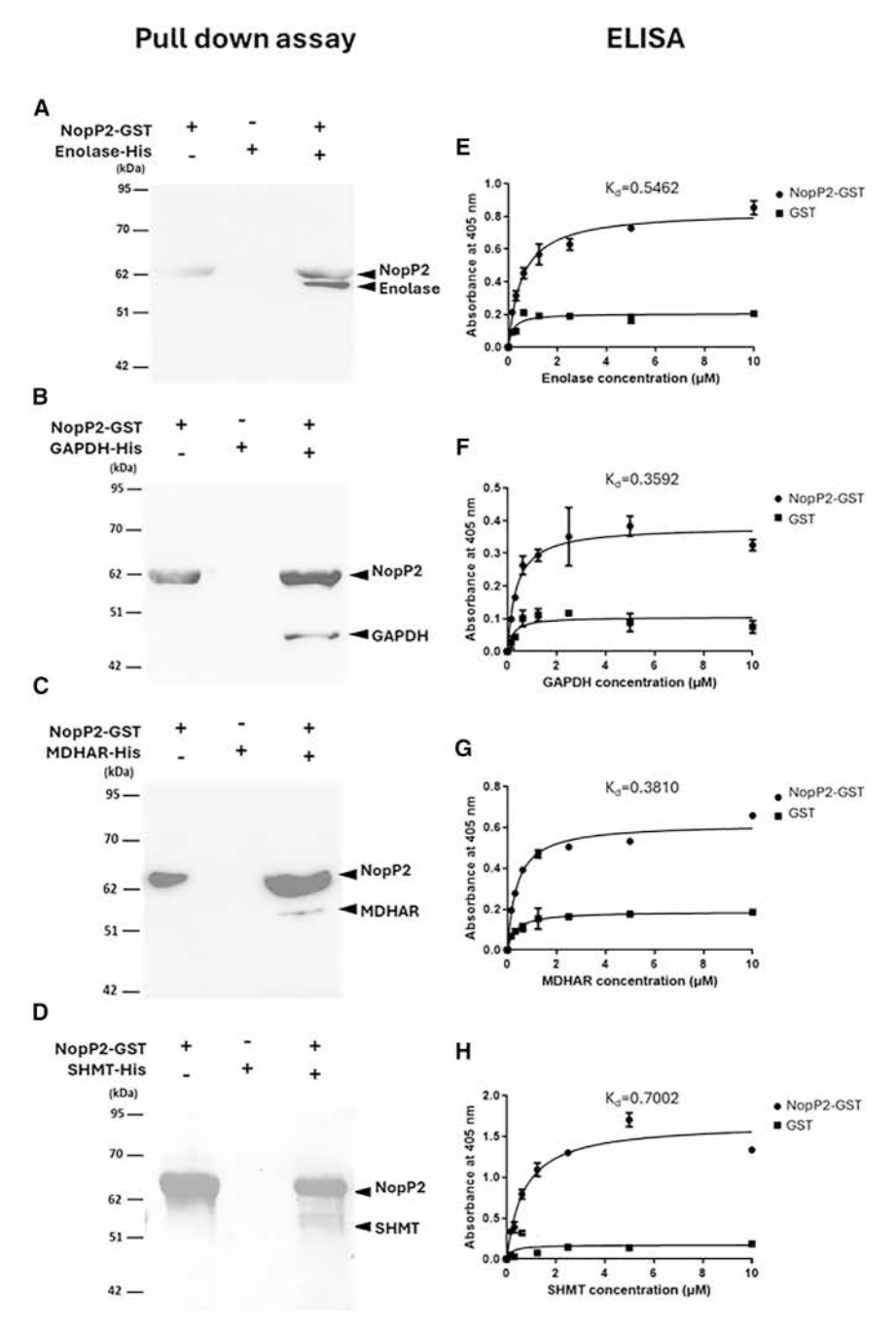
Subcellular localization of nodulation outer protein P2 and its interacting proteins in *planta*

To determine the subcellular localization of NopP2 and the four interacting proteins in *planta*, Transgenic roots of *V. radiata* cv. KPS1 expressing NopP2-GFP and each interacting protein (enolase-mCherry, GAPDH-mCherry, MDHAR-mCherry, and SHMT-mCherry) was generated using hairy root transformation. The co-expressed NopP2-GFP and each interacting protein were initially observed under a fluorescence microscope. Roots

expressing NopP2-GFP exhibited green fluorescence similar to the 35S:GFP control. In contrast, roots expressing mCherry fused with interacting proteins exhibited red fluorescence similar to the 35S:mCherry control (Figures S2A–S2C). In co-expressing roots containing NopP2-GFP and individual interacting partner proteins, we observed the co-localization of these complexes within root cells. To specifically detect NopP2-GFP and avoid background autofluorescence in plant cells, immunoblotting with anti-GFP antibodies was used. The results indicated that roots overexpressing NopP2-GFP exhibited subcellular localization throughout the cytoplasm, with accumulation observed around the cytoplasmic membrane and in the nucleus (Figure 5). While co-expressing mCherry fused with each of the interacting proteins alongside nopP2-GFP, we observed their localization at the plasma membrane. This indicates the co-localization of NopP2







with the four interacting proteins in the same region in the mung bean root, as shown in the overlay capture panels (Figure 5).

Moreover, subcellular localization was confirmed in tobacco leaves using an agroinfiltration approach. Consistent with the previous results observed in mung bean root, co-expression of NopP2-GFP and its interacting proteins showed co-localization at the plasma membrane (Figure 6). Interestingly, the subcellular localization of single expressed proteins was significantly altered when co-expressed with NopP2-GFP and its interacting partners. NopP2-GFP alone localized to filamentous actin, the

Figure 4. Confirmation of NopP2-plant protein interactions by pull-down assay and ELISA binding analysis

(A–D) *In vitro* pull-down assay of protein-protein interaction between NopP2 proteins and each interacting partner. The purified 6xHis tagging of enolase (A), glyceraldehyde-3-phosphate dehydrogenase (GAPDH) (B), monodehydroascorbate reductase (MDHAR) (C), and serine hydroxymethyltransferase (SHMT) (D) were assayed for their binding to the NopP2-GST, which binds to glutathione beads. The protein-protein complexes were separated by 12% SDS-PAGE and analyzed by Western blotting using anti-GST antibody for NopP2-GST and anti-His antibody for detecting His-tagging of each interacting partner.

(E–H) Specific-binding analysis between NopP2 and interacting partners by ELISA. The purified NopP2-GST at a concentration of 0–10 $\mu M.$ The apparent dissociation constant (K_d) of NopP2-GST with interacting proteins was determined in the graph.

plasma membrane, and nuclear membrane, but not within the nucleus. In contrast, all interacting proteins localized to both the membrane and the nucleus (Figure S3). However, the co-expression of NopP2 with its interacting proteins resulted in co-localization exclusively at the plasma membrane (Figure 6). These results suggest that the co-localization of NopP2 and its interacting proteins (including enolase, GAPDH, SHMT, and MDHAR) at the plasma membrane may facilitate their physical interaction within plant cells, where this interaction likely occurs and triggers plant symbiosis incompatibility.

Nodulation outer protein P2 induces a multifaceted plant defense response, leading to incompatible symbiosis in *V. radiata*

A comparative transcriptome analysis was conducted to investigate how NopP2 influences gene expression in mung bean roots during the early stages of infection. RNA-seq analysis was performed on non-inocu-

lated roots and roots inoculated with ORS3257 or Ω nopP2 at 2 and 3 dpi (Accession no. PRJNA117951; see in Table S2). The Venn diagram of comparing the DEGs under different conditions revealed that ORS3257 downregulated 109 unique genes compared with the Ω nopP2 mutant, whereas 121 unique genes were up-regulated. Only 15 genes were differentially expressed in both the non-inoculated (NI)/WT and NopP2/WT comparisons, while no downregulated genes and only one up-regulated gene were differentially expressed across all three comparisons (Figure 7A). The volcano plot shows 123 up-regulated (red) and 125 downregulated





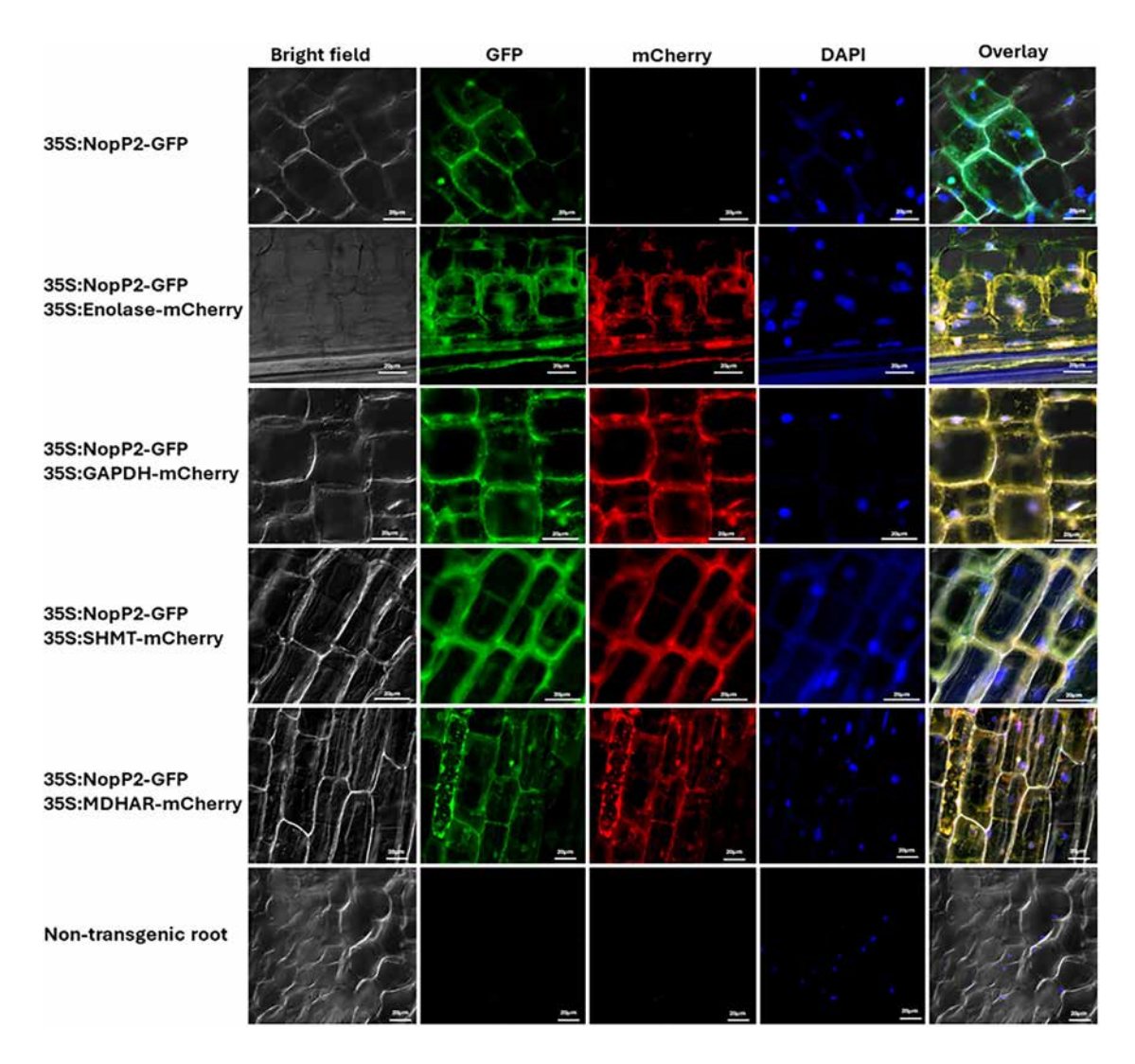


Figure 5. Subcellular localization of NopP2-GFP co-expressed with each interacting protein (Enolase-mCherry, GAPDH-mCherry, SHMT-mCherry, and MDHAR-mCherry) in transgenic *V. radiata* cv. KPS1 root

The images include bright field, green fluorescence for GFP, red fluorescence for mCherry, and blue fluorescence for detecting nuclei via DAPI staining. The overlay images are presented in the last panel. Scale bar: 20 µm.

(blue) genes when comparing the Ω nopP2 mutant strain to the wild-type (ORS3257) strain. Several genes involved in the plant defense response, jasmonic acid/ethylene (JA/ET) response pathways, cell wall modification, photosynthesis, and fatty acid biosynthesis were observed to be up- and downregulated (Figure 7D; Tables S3 and S4). Interestingly, the upregulation of several genes involved in the salicylic acid (SA) response pathway, hypersensitive response, and carbohydrate metabolic process was detected in ORS3257-inoculated roots (Figures 7C and 7D; Tables S3 and S4).

According to RNAseq analysis, genes that were highly up-regulated by ORS3257 and significantly expressed in relation to plant defense and hypersensitive response were also analyzed by using qRT-PCR. The expression of genes encoding pathogenesis-related protein 1 (PR1), thaumatin-like proteins (PR5), transcription factor MYB13, and disease resistance protein TAO1-like was investigated in roots inoculated with ORS3257 and Ω nopP2

at 2 and 3 dpi compared with NI roots. All observed genes were up-regulated in ORS3257 at 2 and 3 dpi, except for MYB13 and TAO1, which were up-regulated only at 2 dpi (Figures 8A–8D). The expression patterns of all genes corresponded with the RNA-seq results (NGS) (Figures 8A–8D). In contrast, the upregulation of symbiotic nodulation genes, including LysM domain receptor-like kinase and early nodulin-75-like (*ENOD75*), was observed in plants inoculated with Ω at 2 and 3 dpi. In comparison, these genes were downregulated in plants inoculated with the ORS3257 strain (Figure S4). These results indicate that NopP2 induces plant defense-related genes, which may inhibit the symbiotic nodulation of ORS3257.

Moreover, the expression of genes corresponding to hypersensitive response, including superoxide dismutase (*SOD*) and peroxidase (*POX10* and *POX16*), were also investigated at 1, 3, and 5 dpi. The results found that *SOD* and *POX10* genes were



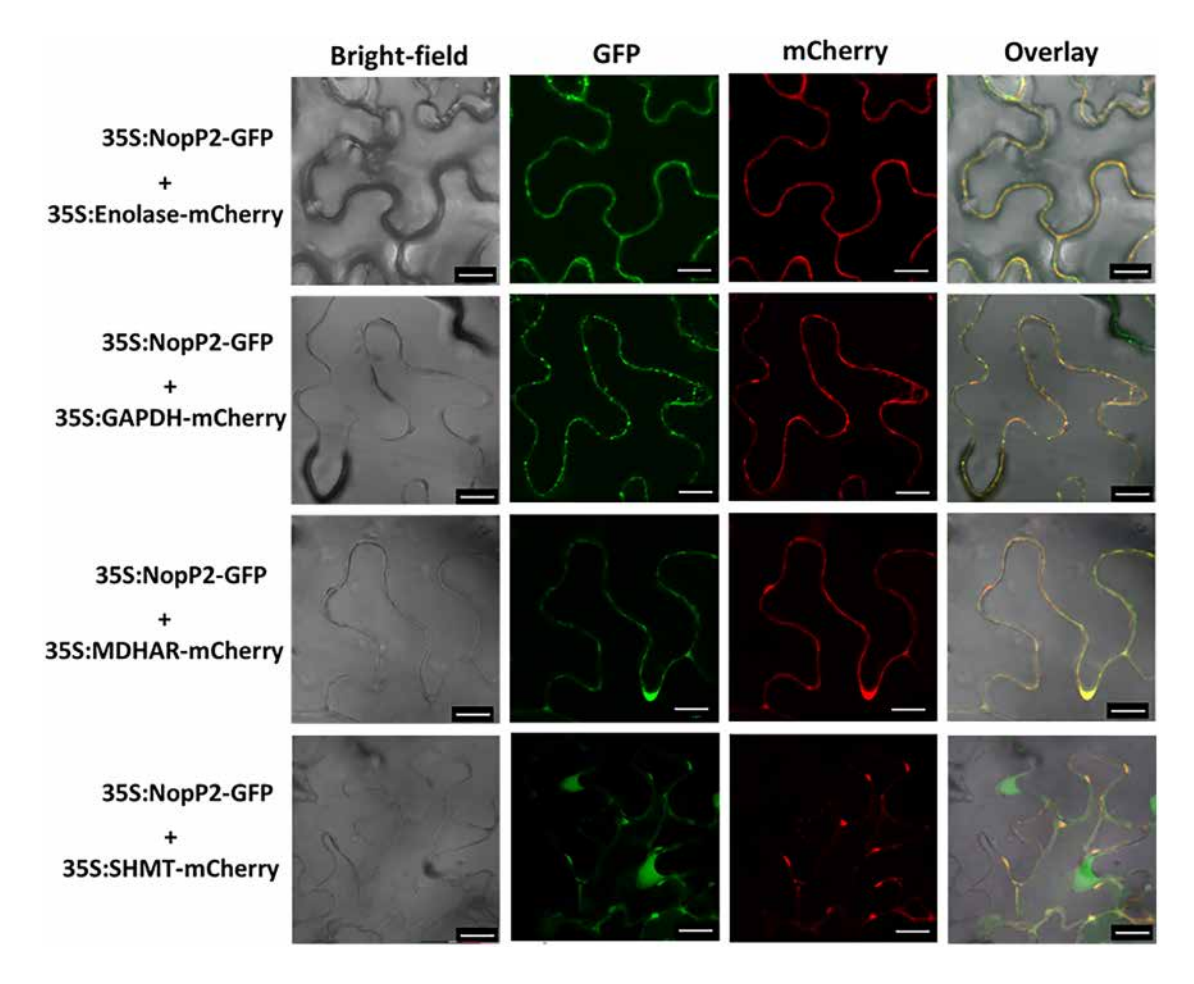


Figure 6. Subcellular localization of NopP2-GFP co-expressed with each interacting protein (Enolase-mCherry, GAPDH-mCherry, SHMT-mCherry, and MDHAR-mCherry) in tobacco leaf epidermal cells was observed 4 days after infiltration

The images include bright field, green fluorescence for GFP, and red fluorescence for mCherry. The overlay images are presented in the last panel. Scale bar: 50 µm.

significantly up-regulated in ORS3257 roots at 1 dpi, while POX10 and POX16 showed high expression in $\Omega nopP2$ roots at 5 dpi (Figures 8F and 8G). However, POX10 and POX16 expression levels observed from RNAseq (NGS) showed significantly up-regulated in ORS3257 roots when compared with $\Omega nopP2$ roots (Figures 8F and 8G). Interestingly, the gene encoding laccase (LAC), which is a key enzyme important for cell wall lignification, showed significant upregulation at both 1 and 5 dpi. This upregulation pattern aligns with the RNAseq result (NGS) (Figure 8H). These results implied that NopP2 from ORS3257 induces the production of oxygen species, peroxidase, and laccase enzymes in the early stage, while later suppressing peroxidase function, leading to H_2O_2 accumulation.

Nodulation outer protein P2 binding may disrupt the activity of interacting proteins without affecting their expression

To elucidate the expression level of the four proteins (enolase, GAPDH, MDHAR, and SHMT) that interact with NopP2, the relative expression of the corresponding genes was observed at 3 and 5 dpi. No significant difference was detected in the expres-

sion of all genes at 3 and 5 dpi, except for enolase and GAPDH, which significantly downregulated expression in ORS3257 roots at 5 dpi. However, RNAseq results (NGS) did not reveal differential expression for any of the interacting partners (Figures 9A–9D). These results suggest that the interaction between NopP2 and its interacting proteins did not affect the expression rates of the four interacting proteins during the early stage of infection.

However, protein-protein interaction can potentially disrupt the function of interacting partners. To investigate this hypothesis, MDHAR activity was measured in roots under different conditions at 5 dpi. The results showed that MDHAR activity was significantly lower in roots inoculated with ORS3257 than in roots inoculated with Ω and NI roots (Figure 9E). This finding confirms that the interaction between NopP2 and MDHAR interferes with MDHAR function, reducing its enzymatic activity without affecting the expression of MDHAR.

Nodulation outer protein P2 triggers hydrogen peroxide accumulation in roots, thereby inhibiting infection

Based on the RNAseq and relative expression results, we speculated that roots inoculated with ORS3257 accumulate H_2O_2 ,



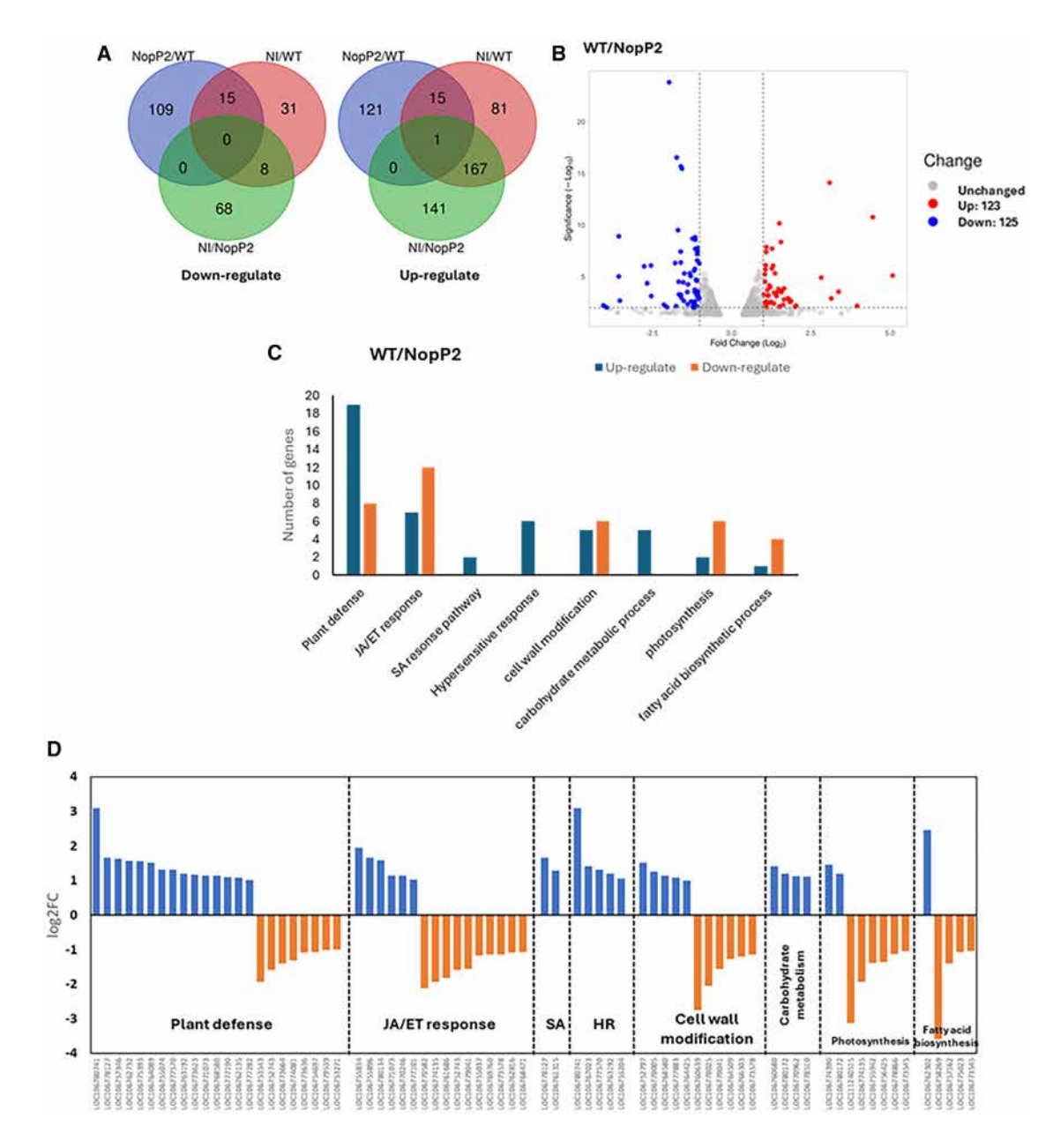


Figure 7. RNA sequencing and GO analysis of V. radiata cv. KPS1 roots after inoculated with ORS3257 (WT) and Ω nopP2 (NopP2) compared with non-inoculated roots (NI)

(A) Venn diagrams of differentially expressed genes (DEGs) which showed upregulated and downregulated by comparing DEGs from NI, WT and Ω nopP2 (NopP2) roots.

(B) Volcano plots analyzed from DEGs results from WT/NopP2. Red points represent up-regulated genes, and blue points represent down-regulated genes $(\text{Log}_2\text{FC of }p\text{-value} > 1 \text{ and } < -1)$ (C) GO functional enrichment analysis of DEGs comparing between ORS3257 (WT) and Ω nopP2 (NopP2). (D) $\text{Log}_2\text{FC of each gene presented from (C) grouped in each function.}$

thereby inhibiting symbiotic nodulation. To test this hypothesis, we examined $\rm H_2O_2$ accumulation in roots inoculated with ORS3257 and $\Omega nopP2$ at 5 dpi, compared with NI roots. As expected, $\rm H_2O_2$ accumulation was detected in roots inoculated with ORS3257, whereas roots infected with $\Omega nopP2$ showed no accumulation, similar to NI roots (Figures 9F–9H). In addition, transgenic roots overexpressing nopP2 (35S:nopP2-GFP) exhibit a high level of $\rm H_2O_2$ accumulation (Figure 9I). These re-

sults suggest that the presence of NopP2 leads to H_2O_2 accumulation in roots, thereby inhibiting infection.

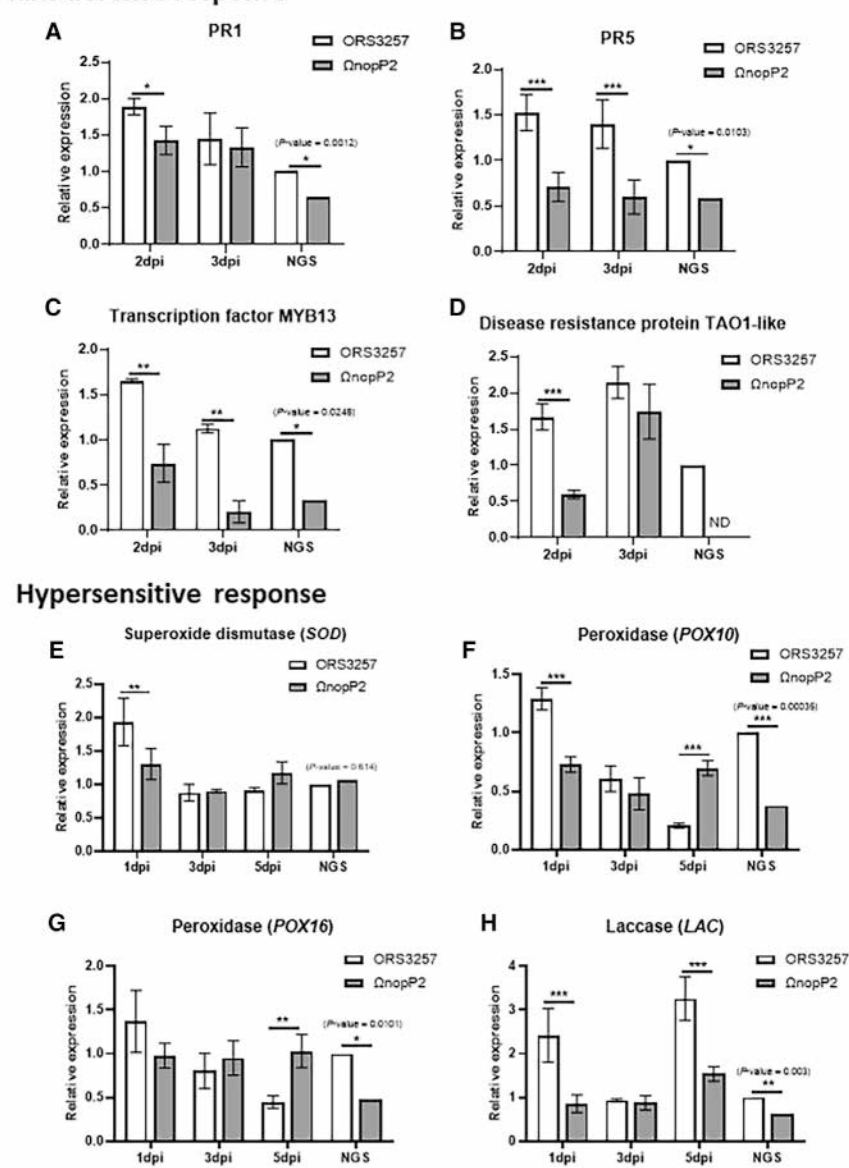
DISCUSSION

Nodule formation and accommodation of symbiotic rhizobia are strictly controlled by the specific recognition and fine-tuned exchange of molecular signals between the host plant and its





Plant defense response



bacterial symbiont during the initiation stage. In addition to NFs, most *Bradyrhizobium* strains, particularly strain ORS3257, use T3SS to deliver a cocktail of effectors that control symbiotic efficiency in *Vigna* species. NopP2 is the most significant factor restricting symbiosis in *V. radiata* (mung bean), as it completely inhibits nodulation in several mung bean cultivars (Figure 1; Table S1). This finding indicates that mung bean may share common interacting proteins specific to NopP2 of ORS3257, thereby rendering the symbiotic incompatibility.

The NopP protein has been identified in several rhizobial strains, but only a subset of these proteins plays a role in symbiotic nodulation. Phylogenetic analysis of the NopP amino acid sequences among rhizobial strains indicates that NopP2 from ORS3257 shares a higher identity with NopP from *B. vignae*

Figure 8. Relative expression of genes involved in the plant defense response (A–D) and hypersensitive response (E–H) in roots inoculated with ORS3257 and Ω nopP2 was analyzed using qRT-PCR

Gene expression levels were normalized to the Actin gene expression and compared to non-inoculated roots as the control. Data represent the mean \pm SD of biological triplicates from two independent experiments, n=6. Statistical analysis was performed using a two-way ANOVA to evaluate the significance of differences (*p<0.05; **p<0.01; ***p<0.001). Additionally, NGS results for ORS3257 and $\Omega nop P2$ were presented in the same graph, with p-values indicated.

and groups closely with NopP from B. elkanii (NopP2 of USDA61) and B. diazoefficiens (such as USDA122 and USDA110) (Figure S5A). However, only NopP from USDA122 has been reported to cause symbiotic incompatibility with Rj2-soybeans and V. radiata cv. KPS1. The protein alignment between the NopP2 sequences of ORS3257 and NopP from USDA122 shows only 72% identity, with many conserved regions in the sequence. Notably, two of the three amino acids in USDA122 NopP that are required for Ri2-soybean incompatibility are not conserved in NopP2 of ORS3257 (Figure S5B). Thus, the mechanism underlying the symbiotic incompatibility of NopP2-ORS3257 may differ from that of NopP-USDA122.

In this study, the introduction of NopP2 from ORS3257 into the effective strain *Bradyrhizobium* sp. SUTN9-2 resulted in lower nodulation efficiency in *V. radiata* KPS2 nodulation compared to the WT strain, indicating that NopP2 negatively interferes with the interaction but does not completely block the symbiosis, contrary to what was observed with

ORS3257. Interestingly, SUTN9-2 contains two NopP homologs in its genome. However, their sequences diverge from NopP2 but are more closely related to NopP1 of ORS3257 and other NopP homologs in other bradyrhizobial strains, which have no reported role in mung bean symbiosis (Figure S5A). Therefore, the presence of two endogenous NopP homologs in SUTN9-2 suggests they likely do not play a significant role in mung bean symbiosis. These phenotypic responses mirrored those previously observed during co-inoculation with ORS3257 and SUTN9-2. Although effective nodule formation was observed in co-inoculated plants, many necrotic nodules were intensively found on the roots, resulting in reduced plant growth compared with SUTN9-2-inoculated plants. ¹⁹ SUTN9-2 may possess positive T3Es or other detoxification systems that counteract the





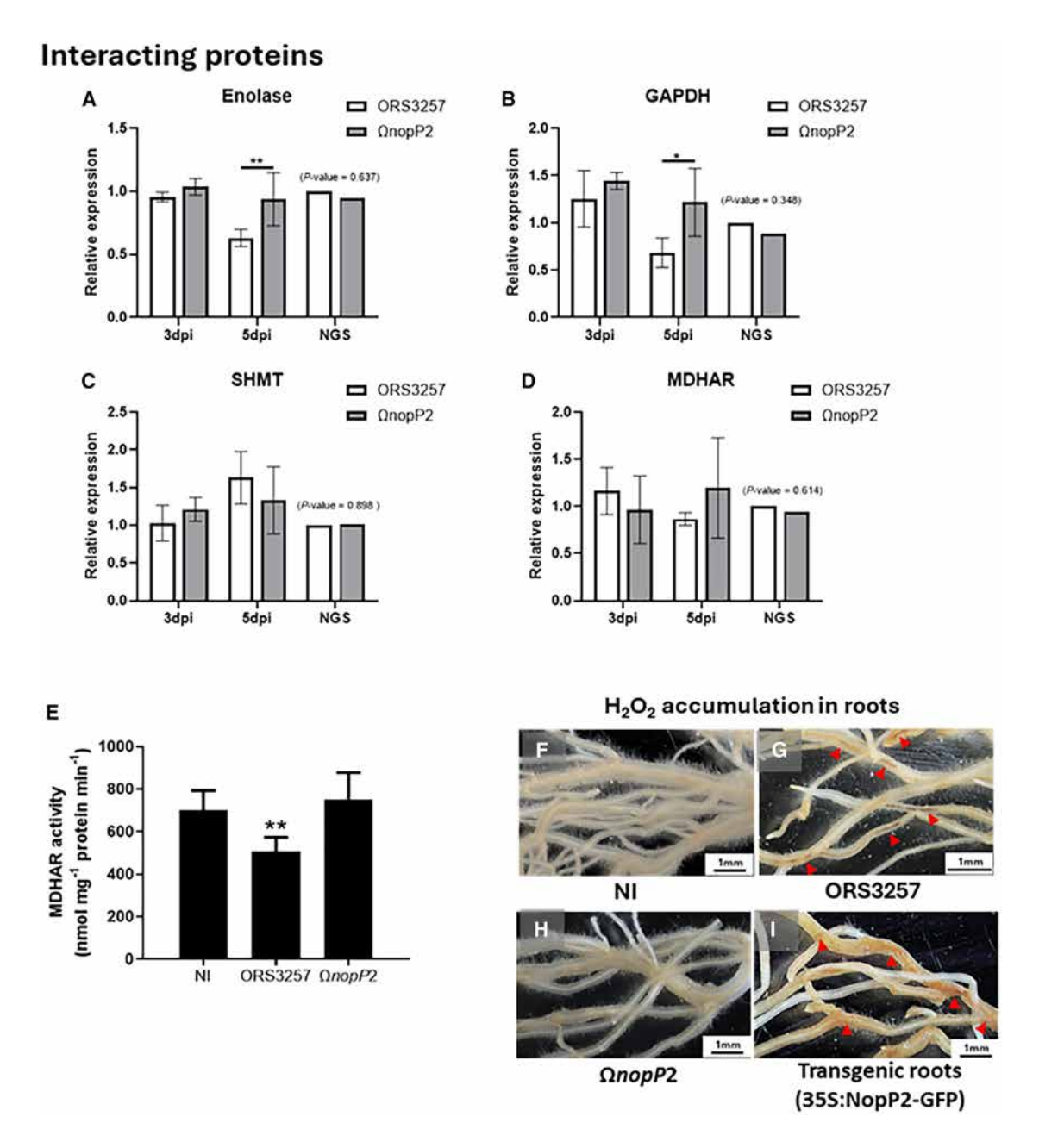


Figure 9. Relative expression of genes of 4 interacting partners of NopP2 (A-D)

The activity of Monodehydroascorbate reductase (MAHAR) of roots with ORS3257 and $\Omega nopP2$ inoculation at 5 dpi compared with non-inoculated roots (NI) (E). Data represent the mean \pm SD of biological triplicates from two independent experiments, n=6. Statistical analysis was performed using a two-way ANOVA to evaluate the significance of differences (*p < 0.05; **p < 0.01; ***p < 0.001). The NGS results for ORS3257 and $\Omega nopP2$ were presented in the same graph, with p-values indicated. The accumulation of H₂O₂ was detected by DAB staining in roots at 5 dpi under different conditions: non-inoculated (F), ORS3257 inoculated (G), $\Omega nopP2$ inoculated (H), and transgenic roots expressing NopP2-GFP (I). The presence of H₂O₂ is indicated by brown staining from the DAB reaction, marked with red arrow heads.

negative effects of NopP2, thereby preventing the plant defense reactions mediated by NopP2 of ORS3257 and maintaining the ability for symbiotic nodulation. However, these findings do not completely exclude the possibility that NopP2 was expressed at a lower level in SUTN9-2, resulting in its reduced secretion in the host cell, or that the added His-tag diminished the functional activity of the NopP2 protein. To investigate this hypothe-

sis, we compared the relative of *nopP2* copy number in the complemented SUTN9-2 strain (9-2+*nopP2*) with that of ORS3257. The results revealed a high quantity of *nopP2* copies in ORS3257 under non-inducing conditions, which was further upregulated in the presence of genistein. In contrast, the complemented SUTN9-2 (9-2+nopP2) also showed an increase in *nopP2* quantity when induced with genistein, while non-induced





9-2+nopP2 remained lower than that observed in ORS3257 (Figure S6A). These findings suggest that the low level of nopP2 expression in SUTN9-2 prior to induction may enable this strain to evade the detrimental effects of NopP2, thereby facilitating symbiotic nodulation.

These expression results are consistent with the protein secretion patterns observed in ORS3257 and 9-2+nopP2 (Figure S6B). The secretome derived from ORS3257 exhibited an NopP2 protein band in both cultures with and without genistein induction. These findings suggest that ORS3257 likely maintains an active T3SS function, which may effectively inhibit symbiotic nodulation during the early stages of infection.

While flavonoids are commonly recognized as inducers of T3SS gene expression through the transcriptional regulator NodD and the specific activator Ttsl, other rhizobia, such as *Cupriavidus taiwanensis*, have shown that T3SS expression can be induced by glutamate instead of flavonoids. ²⁰ This suggests that various environmental signals can trigger T3SS activity in certain rhizobial species. Furthermore, the regulation of T3SS in some plant-beneficial or pathogenic bacteria is primarily influenced by environmental signals and specific transcription factors. ²¹ Therefore, it is possible that the T3SS in ORS3257 may be regulated by multiple factors beyond mere flavonoid presence, potentially involving other environmental signals or internal cellular states that have yet to be elucidated.

Interestingly, the ectopic expression of nopP2 in transformed V. radiata cv. KPS1 roots also contribute to nodulation incompatibility by $\Omega nopP2$ strain, which typically forms active nodules on mung bean roots (Figures 2M and 2N). These results confirm that NopP2 mediates symbiotic incompatibility within the plant. However, transgenic roots with overexpressed nopP2 displayed stunted growth and extensive browning, suggesting cellular damage (Figures 2K-2M and S2B). This phenotype likely reflects a plant defense response triggered by NopP2 interactions within plant cells. In contrast, the overexpression of the positive effector Sup3 from Bradvrhizobium sp. NAS96.2 in the roots of Aeschynomene indica and A. evenia induces spontaneous nodule formation.²² Thus, the simultaneous expression of bacterial effectors in legume roots is a valuable strategy for identifying the specific roles of these effectors in mediating the symbiotic phenotype.

The establishment of symbiotic nodules in legumes is not only controlled by bacterial effectors but also depends on plant proteins that specifically recognize signaling molecules secreted by bacteria. This symbiotic interaction, known as protein-protein interaction, controls the symbiotic compatibility. 23,24 To gain a deeper understanding of the molecular mechanisms underlying this protein-protein interaction, we investigated the interacting proteins of NopP2. We identified four proteins that interact with NopP2: enolase, glyceraldehyde-3-phosphate dehydrogenase (GAPDH), serine hydroxymethyltransferase (SHMT), and monodehydroascorbate reductase (MDHAR). The protein-protein interaction between NopP2 and each protein partner was confirmed by an in vitro pull-down assay and ELISA, suggesting that all partners were in physical interaction and directly bound to the NopP2 protein. Moreover, the results of subcellular localization studies of NopP2 and its interacting proteins, observed in both transgenic mung bean roots and tobacco leaf epidermal cells, confirmed their co-localization at the plasma membrane (Figures 5 and 6). This finding suggests that the co-localization of NopP2 and its interacting proteins at the membrane may facilitate their interactions within the cells, potentially triggering symbiotic incompatibility during their interaction.

Enolase is a glycolytic enzyme that catalyzes the interconversion of 2-phosphoglycerate (2-PG) to phosphoenolpyruvate (PEP), playing a crucial role in glycolysis and various cellular processes²⁵ GAPDH, a glycolytic enzyme, plays a vital role in energy production by converting glyceraldehyde-3-phosphate to 1,3bisphosphoglycerate.²⁶ SHMT is a key enzyme in one-carbon metabolism, crucial for nucleotide synthesis and cell proliferation, as it catalyzes the conversion of serine to glycine and tetrahydrofolate to 5,10-methylene tetrahydrofolate.²⁷ MDHAR functions within the antioxidant defense system, maintaining cellular redox balance by regenerating ascorbate, an important antioxidant, from its oxidized form. 28,29 Interestingly, all NopP2interacting proteins are crucial enzymes involved in cellular metabolism and the antioxidant defense system, which are essential for plant cell survival. Thus, the interaction of these proteins with NopP2 likely disrupts their function rather than activating them. Several studies have shown that the enzymatic inhibition of these proteins can trigger plant immune responses. For example, disrupting enolase activity in A. thaliana enhances pathogen resistance by inducing the expression of the plant defense gene PR1 and increasing the accumulation of hydrogen peroxide (H_2O_2) .³⁰

Similarly, knocking out the GADPH gene leads to increased basal reactive oxygen species (ROS) accumulation under stress conditions, particularly under biotic and abiotic stress.²⁶ SHMT mutations in Arabidopsis similarly lead to H₂O₂ accumulation in leaves, affecting their ability to manage oxidative stress and resulting in chlorotic and necrotic symptoms. 27,31,32 The results of transcriptome analysis and qRT-PCR in this study were consistent with those of previous reports. Roots inoculated with ORS3257 induced the expression of several plant defense genes, including PR1 and PR5 (Figures 8A and 8B). Additionally, genes involved in hypersensitive responses, including superoxide dismutase (SOD) and peroxidase (POX10), were significantly up-regulated at 1 dpi (Figures 8E-8G). These findings supported the observed accumulation of H2O2 in roots inoculated with ORS3257 and transgenic roots expressing NopP2 (Figures 9G and 9I). Our findings also revealed that ORS3257 inoculation induced the expression of LAC genes (encodes laccase enzyme) at 1 and 5 dpi (Figure 8H). Laccase and peroxidase enzymes are essential for lignin polymerization, a process that strengthens plant cell walls by oxidizing phenolic compounds such as lignin monomers.33 These results suggest that NopP2 from ORS3257 triggers the early lignification of the cell wall during infection, potentially hindering the establishment of symbiotic nodulation.

Moreover, this study found that MDHAR is an interacting partner of NopP2. MDHAR is a crucial enzyme that scavenges ROS and protects plant cells against oxidative stress.³⁴ Thus, the interaction between NopP2 and MDHAR may inhibit MDHAR activity and disrupt its protective role, leading to the accumulation of its substrate (MDHA) and a depletion of the ascorbate pool, which results in elevated ROS levels.²⁹ Consistent with this



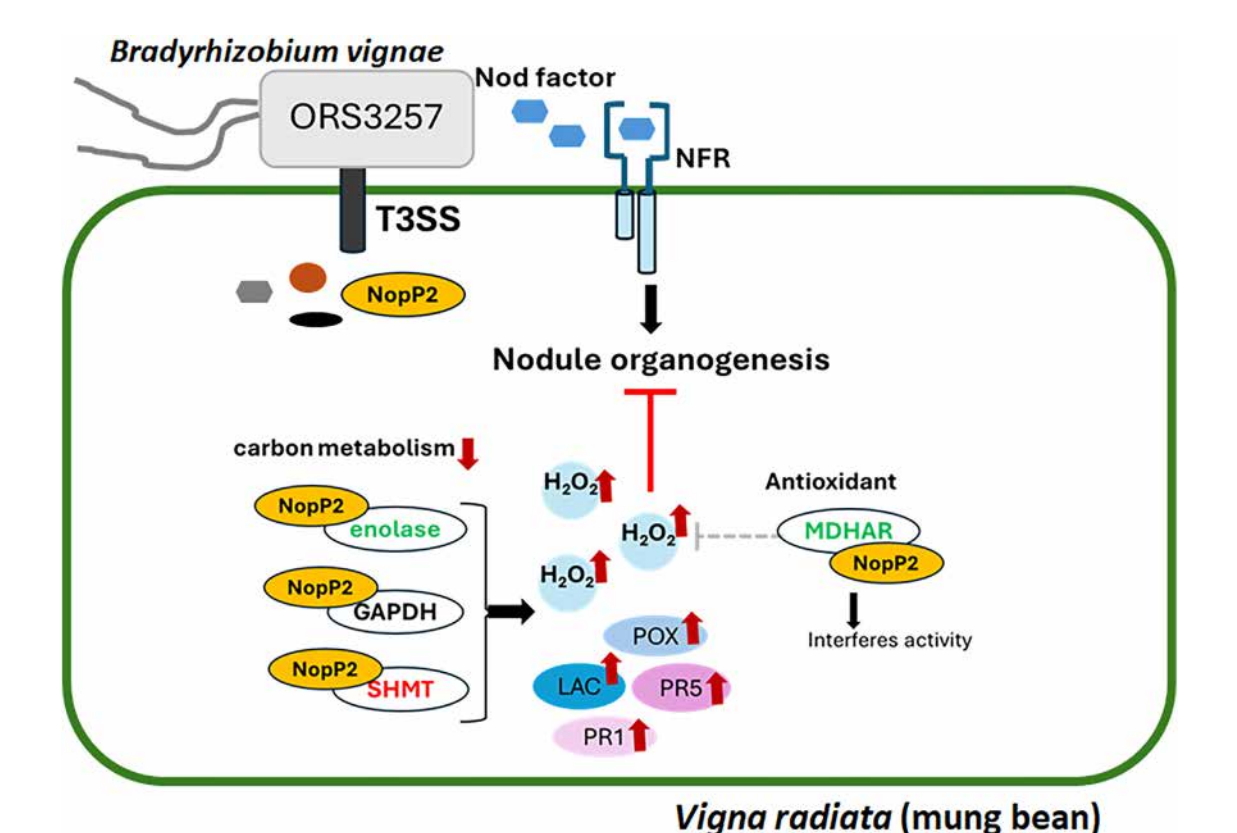


Figure 10. Schematic mechanisms of symbiotic incompatibility by NopP2 of *B. vignae* ORS3257

In addition to initiating nodulation via the Nod-factor pathway, ORS3257 secretes NopP2 through the Type III Secretion System (T3SS). NopP2 directly interacts with enolase, GAPDH, SHMT, and MDHAR, leading to the enhanced expression of several plant defense genes, such as PR1, PR5, POX, and LAC, and increased accumulation of H_2O_2 in roots. These combined reactions ultimately inhibit nodule formation by ORS3257.

evidence, our results showed a decrease in MDHAR activity in roots inoculated with ORS3257, whereas non-inoculated roots and roots with Ω nopP2 maintained similar activity levels to NI roots (Figure 9E). Interestingly, a study on rice demonstrated that disrupting the OsMDHAR4 gene abolished the MDHAR activity. However, this surprisingly enhanced stress tolerance is achieved by altering the cellular redox state and ROS levels. 35

Our findings regarding NopP2 incompatibility in mung bean, a crucial Asian crop valued for its nutrition, economic benefits, and nitrogen-fixing symbiosis with rhizobia. Therefore, the identification of NopP2 interacting proteins and the molecular mechanisms of nodulation host restriction in this study could help over-

come the limitations of biofertilizers caused by NopP2. This knowledge has the potential to significantly improve the efficiency of legume-rhizobium symbiosis in agricultural practices, potentially leading to increased crop yields and improved sustainability.

Limitations of the study

This study provides significant insights into the molecular mechanisms underlying the symbiotic incompatibility between *B. vignae* ORS3257 and *V. radiata* mediated by the effector protein NopP2. However, the research was conducted using a single cultivar of *V. radiata* (cv. KPS1). Different cultivars may exhibit varying responses to NopP2, and the findings may not be universally applicable to all *V. radiata* cultivars. Expanding the research to include multiple cultivars and species would provide a broader perspective on the symbiotic incompatibility mechanisms. Additionally, the validation of the molecular interactions between NopP2 and its target enzymes through *in vivo* studies is required to strengthen the evidence for the proposed mechanisms.

RESOURCE AVAILABILITY

Lead contact

The relevant experimental reagents, experimental methods, and related data of this study can be obtained by contacting Neung Teaumroong (neung@sut.ac.th).





Materials availability

This study did not generate new unique reagents.

Data and code availability

- All data reported in this article will be shared by the lead contact upon request.
- This article does not report original code.
- Any additional information required to reanalyze the data reported in this
 article is available from the lead contact upon request.

ACKNOWLEDGMENTS

This work was supported by (i) National Research Council of Thailand (NRTC) and Suranaree University of Technology (grant number NRCT5-TRG006), (ii) NSRF via the Program Management Unit for Human Resources & Institutional Development, Research, and Innovation (PMU-B) (grant number B13F660067), (iii) JSPS-NRCT by National Research Council of Thailand (grant number N11A670769), (iv) The Office of the Permanent Secretary of the Ministry of Higher Education, Science, Research and Innovation. (v) Suranaree University of Technology (SUT), (vi) Thailand Science Research and Innovation (TSRI), and (vii) National Science, Research, and Innovation Fund (NSRF) (grant number 195582).

AUTHOR CONTRIBUTIONS

Conceptualization: Y.K., E.G., N.B., P.T., S.S, S.O., and N.T.; methodology: P.S. and P.B., validation: P.S., N.P., K.T., S.H., N,H., and M.A.; data curation: P.S., P.P., J.W., and T.K.; formal analysis: P.S., M.A., S.H., N.H., P.P., J.W., and T.K.; investigation: P.S., P.B., N.P., and K.T.; resource: S.O., S.S., Y.K., and E.G.; writing-original draft preparation: P.S. and N.P.; writing-editing: P.S., S.S., Y.K., P.T., E.G., and N.T.; visualization: P.S. and P.B.; supervision: P.T., N.B., and N.T.; project administration: N.T. and P.T.; funding acquisition: N.T. and P.T.; All authors have read and agreed to the published version of the article

DECLARATION OF INTERESTS

The authors declare no competing interests.

STAR*METHODS

Detailed methods are provided in the online version of this paper and include the following:

- KEY RESOURCES TABLE
- EXPERIMENTAL MODEL AND STUDY PARTICIPANT DETAILS
 - o Bacterial strains and culture conditions
 - O Complementation of nopP2 in Bradyrhizobium sp. SUTN9-2
 - Overexpression of NopP2 in mung bean roots
- METHOD DETAILS
 - O Plant nodulation and symbiosis analyses
 - $\, \circ \,$ Extraction and analysis of secreted proteins
 - Relative nopP2 copy number in B. vignae ORS3257 and complemented SUTN9-2 strains
 - Identification of NopP2 interacting target proteins
 - MALDI-TOF MS/MS analysis
 - Confirmation of protein-protein interaction
 - O Subcellular localization in planta
 - o Transcriptome analysis and qRT-PCR
 - MDHAR activity and hydrogen peroxide (H₂O₂) accumulation in roots
 - O Phylogenetic tree construction and protein alignment
- QUANTIFICATION AND STATISTICAL ANALYSIS
 - Quantification for RNA-seq
 - Statistical analysis

SUPPLEMENTAL INFORMATION

Supplemental information can be found online at https://doi.org/10.1016/j.isci. 2025.112351.

Received: July 9, 2024 Revised: October 24, 2024 Accepted: March 11, 2025 Published: April 4, 2025

REFERENCES

- Oldroyd, G.E.D. (2013). Speak, friend, and enter: signalling systems that promote beneficial symbiotic associations in plants. Nat. Rev. Microbiol. 11, 252–263. https://doi.org/10.1038/nrmicro2990.
- Kambara, K., Ardissone, S., Kobayashi, H., Saad, M.M., Schumpp, O., Broughton, W.J., and Deakin, W.J. (2009). Rhizobia utilize pathogen-like effector proteins during symbiosis. Mol. Microbiol. 71, 92–106.
- Staehelin, C., and Krishnan, H.B. (2015). Nodulation outer proteins: double-edged swords of symbiotic rhizobia. Biochem. J. 470, 263–274.
- Teulet, A., Camuel, A., Perret, X., and Giraud, E. (2022). The Versatile Roles of Type III Secretion Systems in *Rhizobium*-Legume Symbioses. Annu. Rev. Microbiol. 76, 45–65. https://doi.org/10.1146/annurev-micro-041020-032624.
- Yuan, M., Jiang, Z., Bi, G., Nomura, K., Liu, M., Wang, Y., Cai, B., Zhou, J.M., He, S.Y., and Xin, X.F. (2021). Pattern-recognition receptors are required for NLR-mediated plant immunity. Nature 592, 105–109. https://doi.org/10.1038/s41586-021-03316-6.
- Ngou, B.P.M., Ahn, H.K., Ding, P., and Jones, J.D.G. (2021). Mutual potentiation of plant immunity by cell-surface and intracellular receptors. Nature 592, 110–115. https://doi.org/10.1038/s41586-021-03315-7.
- Songwattana, P., Chaintreuil, C., Wongdee, J., Teulet, A., Mbaye, M., Piromyou, P., Gully, D., Fardoux, J., Zoumman, A.M.A., Camuel, A., et al. (2021). Identification of type III effectors modulating the symbiotic properties of *Bradyrhizobium vignae* strain ORS3257 with various *Vigna* species. Sci. Rep. 11, 4874. https://doi.org/10.1038/s41598-021-84205-w.
- Xin, D.-W., Liao, S., Xie, Z.-P., Hann, D.R., Steinle, L., Boller, T., and Staehelin, C. (2012). Functional analysis of NopM, a novel E3 ubiquitin ligase (NEL) domain effector of *Rhizobium* sp. strain NGR234. PLoS Pathog. 8, e1002707.
- Piromyou, P., Nguyen, H.P., Songwattana, P., Boonchuen, P., Teamtisong, K., Tittabutr, P., Boonkerd, N., Alisha Tantasawat, P., Göttfert, M., Okazaki, S., and Teaumroong, N. (2021). The *Bradyrhizobium diazoefficiens* type III effector NopE modulates the regulation of plant hormones towards nodulation in *Vigna radiata*. Sci. Rep. 11, 16604. https://doi.org/10.1038/s41598-021-95925-4.
- Jiménez-Guerrero, I., Medina, C., Vinardell, J.M., Ollero, F.J., and López-Baena, F.J. (2022). The Rhizobial Type 3 Secretion System: The Dr. Jekyll and Mr. Hyde in the *Rhizobium*–Legume Symbiosis. Int. J. Mol. Sci. 23, 1108. https://doi.org/10.3390/ijms231911089.
- Skorpil, P., Saad, M.M., Boukli, N.M., Kobayashi, H., Ares-Orpel, F., Broughton, W.J., and Deakin, W.J. (2005). NopP, a phosphorylated effector of *Rhizobium* sp. strain NGR234, is a major determinant of nodulation of the tropical legumes *Flemingia congesta* and *Tephrosia vogelii*. Mol. Microbiol. 57, 1304–1317.
- Ausmees, N., Kobayashi, H., Deakin, W.J., Marie, C., Krishnan, H.B., Broughton, W.J., and Perret, X. (2004). Characterization of NopP, a type III secreted effector of *Rhizobium* sp. strain NGR234. J. Bacteriol. 186, 4774–4780.
- Sugawara, M., Takahashi, S., Umehara, Y., Iwano, H., Tsurumaru, H., Odake, H., Suzuki, Y., Kondo, H., Konno, Y., Yamakawa, T., et al. (2018). Variation in bradyrhizobial NopP effector determines symbiotic incompatibility with Rj2-soybeans via effector-triggered immunity. Nat. Commun. 9, 3139.



- Liu, Y., Lin, Y., Wei, F., Lv, Y., Xie, F., Chen, D., Lin, H., and Li, Y. (2023). G-type receptor-like kinase AsNIP43 interacts with rhizobia effector nodulation outer protein P and is required for symbiosis. Plant Physiol. 193, 1527–1546. https://doi.org/10.1093/plphys/kiad318.
- Jiménez-Guerrero, I., Pérez-Montaño, F., Medina, C., Ollero, F.J., and López-Baena, F.J. (2017). The Sinorhizobium (Ensifer) fredii HH103 nodulation outer protein Nopl is a determinant for efficient nodulation of soybean and cowpea plants. Appl. Environ. Microbiol. 83, e02770-16. https://doi.org/10.1128/AEM.02770-16.
- Jiménez-Guerrero, I., Acosta-Jurado, S., Medina, C., Ollero, F.J., Alias-Villegas, C., Vinardell, J.M., Pérez-Montaño, F., and López-Baena, F.J. (2020). The Sinorhizobium fredii HH103 type III secretion system effector NopC blocks nodulation with Lotus japonicus Gifu. J. Exp. Bot. 71, 6043–6056. https://doi.org/10.1093/jxb/eraa297.
- Zhang, B., Wang, M., Sun, Y., Zhao, P., Liu, C., Qing, K., Hu, X., Zhong, Z., Cheng, J., Wang, H., et al. (2021). *Glycine max* NNL1 restricts symbiotic compatibility with widely distributed bradyrhizobia via root hair infection. Nat. Plants 7, 73–86. https://doi.org/10.1038/s41477-020-00832-7.
- Liu, D., Luo, Y., Zheng, X., Wang, X., Chou, M., and Wei, G. (2021). TRAPPC13 is a novel target of *Mesorhizobium amorphae* type III secretion system effector NopP. Mol. Plant Microbe Interact. 34, 511–523. https:// doi.org/10.1094/MPMI-12-20-0354-FI.
- Piromyou, P., Songwattana, P., Teamtisong, K., Tittabutr, P., Boonkerd, N., Tantasawat, P.A., Giraud, E., Göttfert, M., and Teaumroong, N. (2019). Mutualistic co-evolution of T3SSs during the establishment of symbiotic relationships between *Vigna radiata* and Bradyrhizobia. Microbiologyopen 8, e00781. https://doi.org/10.1002/mbo3.781.
- Saad, M.M., Crèvecoeur, M., Masson-Boivin, C., and Perret, X. (2012). The type 3 protein secretion system of *Cupriavidus taiwanensis* strain LMG19424 compromises symbiosis with *Leucaena leucocephala*. Appl. Environ. Microbiol. 78, 7476–7479. https://doi.org/10.1128/AEM. 01691-12.
- Zboralski, A., Biessy, A., and Filion, M. (2022). Bridging the Gap: Type III Secretion Systems in Plant-Beneficial Bacteria. Microorganisms 10, 187. https://doi.org/10.3390/microorganisms10010187.
- Camuel, A., Teulet, A., Carcagno, M., Haq, F., Pacquit, V., Gully, D., Pervent, M., Chaintreuil, C., Fardoux, J., Horta-Araujo, N., et al. (2023). Widespread *Bradyrhizobium* distribution of diverse Type III effectors that trigger legume nodulation in the absence of Nod factor. ISME J. 17, 1416–1429. https://doi.org/10.1038/s41396-023-01458-1.
- Yang, S., Tang, F., Gao, M., Krishnan, H.B., and Zhu, H. (2010). R genecontrolled host specificity in the legume-rhizobia symbiosis. Proc. Natl. Acad. Sci. 107, 18735–18740.
- 24. Flor, H.H. (1971). Current status of the gene-for-gene concept. Annu. Rev. Phytopathol. 9, 275–296.
- Van der Straeten, D., Rodrigues-Pousada, R.A., Goodman, H.M., and Van Montagua, M. (1991). Plant Enolase: Gene Structure, Expression, and Evolution. Plant Cell 3, 719–735.
- Henry, E., Fung, N., Liu, J., Drakakaki, G., and Coaker, G. (2015). Beyond Glycolysis: GAPDHs Are Multi-functional Enzymes Involved in Regulation of ROS, Autophagy, and Plant Immune Responses. PLoS Genet. 11, e1005199. https://doi.org/10.1371/journal.pgen.1005199.
- Fang, C., Zhang, P., Li, L., Yang, L., Mu, D., Yan, X., Li, Z., and Lin, W. (2020). Serine hydroxymethyltransferase localised in the endoplasmic reticulum plays a role in scavenging H₂O₂ to enhance rice chilling tolerance. BMC Plant Biol. 20, 236. https://doi.org/10. 1186/s12870-020-02446-9.
- Dumanović, J., Nepovimova, E., Natić, M., Kuča, K., and Jaćević, V. (2021). The Significance of Reactive Oxygen Species and Antioxidant Defense System in Plants: A Concise Overview. Front Plant Sci. 11, 552969. https://doi.org/10.3389/fpls.2020.552969.
- 29. Rajput, V.D., Harish, Singh, R.K., Verma, K.K., Sharma, L., Quiroz-Figueroa, F.R., Meena, M., Gour, V.S., Minkina, T., Sushkova, S., et al.

- (2021). Recent developments in enzymatic antioxidant defence mechanism in plants with special reference to abiotic stress. Biology (Basel) 10, 267. https://doi.org/10.3390/biology10040267.
- Yang, L., Wang, Z., Zhang, A., Bhawal, R., Li, C., Zhang, S., Cheng, L., and Hua, J. (2022). Reduction of the canonical function of a glycolytic enzyme enolase triggers immune responses that further affect metabolism and growth in *Arabidopsis*. Plant Cell 34, 1745–1767. https://doi.org/10. 1093/plcell/koab283.
- Zhou, H., Zhao, J., Yang, Y., Chen, C., Liu, Y., Jin, X., Chen, L., Li, X., Deng, X.W., Schumaker, K.S., and Guo, Y. (2012). UBIQUITIN-SPECIFIC PROTEASE16 modulates salt tolerance in arabidopsis by regulating Na+/H+ antiport activity and serine hydroxymethyl-transferase stability. Plant Cell 24, 5106–5122. https://doi.org/10.1105/toc.112.106393.
- Moreno, J.I., Martín, R., and Castresana, C. (2005). Arabidopsis SHMT1, a serine hydroxymethyltransferase that functions in the photorespiratory pathway influences resistance to biotic and abiotic stress. Plant J. 41, 451–463. https://doi.org/10.1111/j.1365-313X. 2004.02311.x.
- Hoffmann, N., Benske, A., Betz, H., Schuetz, M., and Samuels, A.L. (2020). Laccases and peroxidases co-localize in lignified secondary cell walls throughout stem development. Plant Physiol. 184, 806–822. https://doi. org/10.1104/pp.20.00473.
- 34. Park, A.K., Kim, I.S., Do, H., Jeon, B.W., Lee, C.W., Roh, S.J., Shin, S.C., Park, H., Kim, Y.S., Kim, Y.H., et al. (2016). Structure and catalytic mechanism of monodehydroascorbate reductase, MDHAR, from *Oryza sativa* L. japonica. Sci. Rep. 6, 33903. https://doi.org/10.1038/srep33903.
- Liu, J., Sun, X., Xu, F., Zhang, Y., Zhang, Q., Miao, R., Zhang, J., Liang, J., and Xu, W. (2018). Suppression of OsMDHAR4 enhances heat tolerance by mediating H₂O₂-induced stomatal closure in rice plants. Rice 11, 38. https://doi.org/10.1186/s12284-018-0230-5.
- Callow, J.A. (1971). A Manual for the Practical Study of Root-Nodule Bacteria (JSTOR).
- Sambrook, J., Fritsch, E.F., and Maniatis, T. (2001). Molecular Cloning: A Laboratory Manual, 2nd, ed.
- Sarapat, S., Longtonglang, A., Umnajkitikorn, K., Girdthai, T., Boonkerd, N., Tittabutr, P., and Teaumroong, N. (2020). Application of rice endophytic *Bradyrhizobium* strain SUTN9-2 containing modified ACC deaminase to rice cultivation under water deficit conditions. J. Plant Interact. 15, 322–334.
- Somasegaran, P., and Hoben, H.J. (1994). Handbook for Rhizobia: Methods in Legume-Rhizobium Technology.
- Ehrhardt, D.W., Atkinson, E.M., and Long, S.R. (1992). Depolarization of alfalfa root hair membrane potential by *Rhizobium meliloti* Nod factors. Science 256, 998–1000.
- Bonaldi, K., Gherbi, H., Franche, C., Bastien, G., Fardoux, J., Barker, D., Giraud, E., and Cartieaux, F. (2010). The Nod Factor-Independent Symbiotic Signaling Pathway Development of Agrobacterium rhizogenes-Mediated Transformation for the Legume Aeschynomene indica. MPMI (Mol. Plant-Microbe Interact.) 23, 1537– 1544. https://doi.org/10.1094/MPMI.
- Kusakabe, S., Higasitani, N., Kaneko, T., Yasuda, M., Miwa, H., Okazaki, S., Saeki, K., Higashitani, A., and Sato, S. (2020). Lotus accessions possess multiple checkpoints triggered by different type III secretion system effectors of the wide-host-range symbiont *Bradyrhizobium elkanii* USDA61. Microbes Environ. 35, ME19141. https://doi.org/10.1264/jsme2.ME19141.
- Eble, J.A. (2018). Titration ELISA as a method to determine the dissociation constant of receptor ligand interaction. JoVE J. 132, 57334. https:// doi.org/10.3791/57334.
- Zhou, Y., Liu, H., Wu, T., Zheng, Y., Wang, R., Xue, D., Yan, Q., Yuan, X., and Chen, X. (2023). Screening of Reference Genes under Biotic





- Stress and Hormone Treatment of Mung Bean (*Vigna radiata*) by Quantitative Real-Time PCR. Genes *14*, 1739. https://doi.org/10.3390/genes14091739.
- Libik-Konieczny, M., Kozieradzka-Kiszkurno, M., Desel, C., Michalec-Warzecha, Ż., Miszalski, Z., and Konieczny, R. (2015). The localization of NADPH oxidase and reactive oxygen species in in vitro-cultured *Mesem*-
- bryanthemum crystallinum L. hypocotyls discloses their differing roles in rhizogenesis. Protoplasma 252, 477–487. https://doi.org/10.1007/s00709-014-0692-2.
- Corpet, F. (1988). Multiple sequence alignment with hierarchical clustering. Nucleic Acids Res. 16, 10881–10890. https://doi.org/10.1093/nar/16.22.10881.



STAR***METHODS**

KEY RESOURCES TABLE

REAGENT or RESOURCE	SOURCE	IDENTIFIER	
Antibodies			
Mouse anti-GST	Abbkine, USA	Cat# ABT2030; RRID:AB_141944	
Goat anti-mouse conjugated HRP	Abbkine, USA	Cat# A21010; RRID:AB_11211441	
Mouse anti-HIS	Abbkine, USA	Cat# ABT2050; RRID:AB_2801388	
Goat anti-mouse conjugated with Alexa Fluor 488	Thermo Scientific [™] ,USA	Cat# A-11001; RRID:AB_1500907	
Mouse anti-GFP	Abbkine, USA	Cat# ABT2020; RRID:AB_10750326	
Bacterial and virus strains			
Agrobacterium rhizogenes strain K599	Lifeasible	Cat# ACC-121	
Agrobacterium tumefaciens strain AGL1	GOLDBIO	Cat# CC-208-A	
Escherichia coli DH5α	Takara	Cat# 9057	
E. coli BL21 (DE3)	Takara	Cat# 9126	
Chemicals, peptides, and recombinant proteins			
Cefotaxime Sodium Salt	Sigma-Aldrich, USA	Cat#501786399	
Kanamycin	Thermo Scientific TM ,USA	Cat#BP906-5	
Ampicillin	Sigma-Aldrich, USA	Cat#A9518	
DAPI (4',6-diamidino-2-phenylindole, dihydrochloride)	Thermo Scientific TM ,USA	Cat#PI62247	
Driselase	Sigma-Aldrich, USA	Cat#D8037	
NADH	Sigma-Aldrich, USA	Cat#481972	
ascorbate	Supelco, Merck, USA	Cat#47863	
ascorbate oxidase	Sigma-Aldrich, USA	Cat#A0157	
DAB (3,3'-diaminobenzidine tetrachloride)	Sigma-Aldrich, USA	Cat#D5637	
Genistein	Sigma-Aldrich, USA	Cat# G6776	
Critical commercial assays			
DC protein assay kits	Bio-Rad, USA	Cat#5000111	
Amersham ECL Western Blotting Detection Reagent	Cytiva, USA	Cat# RPN3004	
FavorPrep Plant Total RNA Purification Mini Kit	Favorgen, Taiwan	Cat#FAPRK 001-2	
iScript [™] cDNA Synthesis Kit	Bio-Rad, USA	Cat#1708890	
Luna® Universal qPCR Master Mix	NEB, USA	Cat#M3003E	
Ni-NTA agarose beads	Qiagen, Germany	Cat#30210	
Glutathione beads 4FF	Bio Basic Asia Pacific, Singapore	Cat#SA010025	
5–20% gradient gel, e-PAGEL	ATTO, Japan	Cat#2331730	
Coomassie Brilliant Blue R-250 staining solution	Bio-Rad, USA	Cat# #1610435	
Deposited data			
RNA-seq (also see in Table S2)	NCBI	BioProject ID: PRJNA1179513	
Experimental models: Organisms/strains			
Wild-type strain <i>Bradyrhizobium vignae</i> ORS3257	Songwattana et al. ⁷	ORS3257	
ORS3257 derivative mutant of main genes encoding components of the T3SS apparatus deleted via double crossing-over, Cefo ^r	Songwattana et al. ⁷	ΔT3SS	
A genetically modified ORS3257 strain contains a segment of plasmid pVO155-npt2-GFP-npt2-Cefo inserted within its nopP2 gene, Cefo ^r , Km ^r	Songwattana et al. ⁷	ΩπορΡ2	
Wild-type strain <i>Bradyrhizobium</i> sp. SUTN9-2, effective strain for mung bean nodulation	Piromyou et al. ¹⁹	SUTN9-2	

(Continued on next page)





Continued		
REAGENT or RESOURCE	SOURCE	IDENTIFIER
SUTN9-2 derivative complemented with the nopP2 rom ORS3257 with carried on pMG103-npt2-Cefo, Cefo ^r	This paper	9-2+nopP2
Dligonucleotides		
or all construction and qRT-PCR, see Table S6	IDT, Coralville, IA, USA	N/A
Recombinant DNA		
Replicative plasmid containing <i>nopP2</i> gene with its promoter and 6×His tagged at C-terminal, used for lopP2 complementation in strain SUTN9-2, Cefo ^r	This study	pm: <i>nopP2</i> -6xHis-pMG103-nptII-cefo ^r
Recombinant plasmid for overproducing NopP2-His in E. coli BL21 (DE3), Amp ^r	This study	NopP2-6xHis-PET19b
Recombinant plasmid for overproducing NopP2-GST on E. coli BL21 (DE3), Amp ^r	This study	NopP2-GST-pGEX-4T
Recombinant plasmid for overproducing Enolase-His n <i>E. coli</i> BL21 (DE3), Amp ^r	This study	Enolase-6xHis-pET22b
Recombinant plasmid for overproducing GAPDH-His n <i>E. coli</i> BL21 (DE3), Amp ^r	This study	GAPDH-6xHis-pET22b
Recombinant plasmid for overproducing MDHAR-His n. E. coli BL21 (DE3), Amp ^r	This study	MDHER-6xHis-pET22b
Recombinant plasmid for overproducing SHMT-His in E. coli BL21 (DE3), Amp ^r	This study	SHMT-6xHis-pET22b
Agrobacterium binary vector for root transformation, bygromycin and kanamycin resistance (Km¹), contains GFP-Tnos under the control of CaMV35S promoter	Abcam, Cat. #ab275760	pCAMBIA1302
Derivative <i>Agrobacterium</i> binary vector pCAMBIA1302 or root transformation, modified by replacing the CaMV35S:mCherry-Tnos fragment to GFP, Km ^r	This study	CaMV35S:mCherry:Tnos-pCAMBIA
Derivative pCAMBIA1302 binary vector for overexpressing NopP2 fused with GFP under the control of CaMV35S promoter, Km ^r	This study	35S:NopP2-GFP
Derivative pCAMBIA1302 binary vector for overexpressing Enolase fused with mCherry under the control of CaMV35S promoter, Km ^r	This study	35S:Enolase:mCherry
Derivative pCAMBIA1302 binary vector for overexpressing GAPDH fused with mCherry under the control of CaMV35S promoter, Km ^r	This study	35S:GAPDH:mCherry
Derivative pCAMBIA1302 binary vector for overexpressing SHMT fused with mCherry under the control of CaMV35S promoter, Km ^r	This study	35S:SHMT:mCherry
Derivative pCAMBIA1302 binary vector for overexpressing MDHAR fused with mCherry under the control of CaMV35S promoter, Km ^r	This study	35S:MDHAR:mCherry
Software and algorithms		
//S-Fit ProteinProspector software	Şekerci et al., 2024	http://prospector.ucsf.edu/
SCIEX TOF/TOF [™] 5800 System	SCIEX, USA	https://sciex.com/products/mass- spectrometers/tof-tof-systems
ProteinPilot Software	SCIEX, USA	https://sciex.com/products/software/ proteinpilot-software
SPSS Statistics for Windows (version 26)	SPSS Inc., Chicago, IL	https://www.ibm.com/support/pages/spss-statistics-v26-now-available
Aultalin program	Corpet, 1988	http://multalin.toulouse.inra.fr/multalincgi-bin/multalin.pl



EXPERIMENTAL MODEL AND STUDY PARTICIPANT DETAILS

Bacterial strains and culture conditions

The bacterial strains used in this study are listed in Table S5. *Bradyrhizobium vignae* ORS3257 and *Bradyrhizobium* sp. SUTN9-2, the derivative mutants of ORS3257, and the complementation of SUTN9-2 were grown in yeast mannitol (YM) medium³⁶ at 30°C on a rotary shaker at 180 rpm for 5 days. The culture media for the derivative mutant or complemented strains were supplemented with 20 μ g/mL cefotaxime (Cefo). *Agrobacterium rhizogenes* strain K599 was used to transform hairy *V. radiata* roots. *Escherichia coli* strain DH5 α was used for cloning, whereas strain BL21 (DE3) was used for protein expression. When required, *A. rhizogenes* and *E. coli* were cultured in Luria-Bertani (LB)³⁷ supplemented with the appropriate antibiotics at the following concentrations: 50 μ g/mL kanamycin (Km), and 100 μ g/mL ampicillin (Amp).

Complementation of nopP2 in Bradyrhizobium sp. SUTN9-2

To determine the effect of NopP2 derived from ORS3257 on nodulation efficiency in the symbiotic effective strain SUTN9-2. The full length of the nopP2 gene with its 500-pb upstream promoter (pm) and 6×His tagging at the C-terminal region (pm:nopP2-6×His; 1,365 bp in total length) were amplified from the ORS3257 genome using specific primers (Table S6). The fragment was directly cloned into pMG103-nptll-cefo^r at the EcoRl/xbal site (namely pm:nopP2-6×His-pMG103-nptll-cefo^r). The constructed plasmid was transformed into SUTN9-2 by electroporation using the BTX GeminiX2 system (Havard Bioscience, Inc.), following the protocol described by Sarapat et al. The transformant was selected in YM medium supplemented with 20 μ g/mL cefotaxime and annotated as 9-2+nopP2.

Overexpression of NopP2 in mung bean roots

The NopP2-overexpressing roots were performed with V. radiata cv. KPS1. Three-day-olds of germinated seeds were injected with A. rhizogenes K599 harboring binary plasmid pCAMBIA1302 and 35S:NopP2-green fluorescent protein (GFP) via needle punching. When the transgenic hairy roots were formed, the plants with transgenic hairy roots were transplanted into new Leonard's jars containing sterilized vermiculite. After 5 days of planting, roots were inoculated with ORS3257 and Ω nopP2 cultures and grown under controlled environmental conditions (28 ± 2°C with a 16 h:8 h of light: dark cycle, light intensities of 300 μ E/m²S, and 70% humidity). The transgenic roots were confirmed by PCR verification using specific primers on the CaMV35S promotor and Nos-terminator region.

METHOD DETAILS

Plant nodulation and symbiosis analyses

The mung bean (V. radiata) cultivars used in this study are listed in Table S1. The seeds were surface sterilized with 70% (V) ethanol for 3 min and then soaked in 3% (V) sodium hypochlorite solution for an additional 5 min. The seeds were then washed with sterilized water five times and germinated on 0.8% water agar plates at 30°C overnight. The germinated seeds were transplanted into Leonard's jars containing sterilized vermiculite³⁹ and watered with minimal buffered nodulation medium (BNM) medium. Plantlets were grown in a controlled environment at 28°C with a 16-h light/8-h dark cycle at 300 μ mol/m²/s light intensity and 70% humidity. Five days after planting, seedlings were inoculated with 1 mL of a 5-day-olds culture adjusted to an OD₆₀₀ of 1 (approximately 10⁹ cells/mL) after cells were washed with sterilized water. Plant phenotypes after 21 days after inoculation (dpi) and nodule number were observed. The dry weights of plants were determined after drying at 65°C for 3 days. The nitrogenase activities were measured using an acetylene reduction assay (ARA) by using Gas chromatography (GC). The experiment was conducted in duplicate using five plants per condition.

Extraction and analysis of secreted proteins

Protein secretion from strain ORS3257 and its derivative mutants (Δ T3SS and Ω nopP2) were extracted following the description from Kusakabe et al. ⁴² Briefly, the bacterial strains were cultured in an Arabinose-gluconate (AG) medium at 28°C to obtain cells at OD₆₀₀ to 0.5. The cultures were induced with 10 μ M genistein (Sigma-Aldrich) (+Gen) and continued for 48 h. The cells were harvested and extracted using Tris-saturated phenol and DTT. The secreted proteins of strain ORS3257 were analyzed by comparison with those in culture without induction (-Gen), whereas all mutant strains were induced with genistein. Five micrograms of secreted proteins from all strains were observed using SDS-PAGE (5–20% gradient gel, e-PAGEL, ATTO) and stained with Coomassie Brilliant Blue R-250 staining solution (Bio-Rad).

Relative nopP2 copy number in B. vignae ORS3257 and complemented SUTN9-2 strains

B. vignae ORS3257 and complemented SUTN9-2 (9-2+*nopP2*) were cultured in AG medium at 28°C until the optical density (OD₆₀₀) reached 0.5. The cultures were then induced with 10 μM genistein (Sigma-Aldrich) (+Gen) and incubated for an additional 48 hours. Following this, the cells were harvested, and total RNA was extracted using the FavorPrepTM Tissue Total RNA Kit (Favorgen, Taiwan). A total of 500 ng of RNA was utilized for cDNA synthesis with the iScriptTM cDNA Synthesis Kit (Bio-Rad), following the manufacturer's instructions. Quantitative real-time PCR (gRT-PCR) was conducted using Luna® Universal qPCR Master Mix (NEB, USA),





with 5 ng of cDNA per reaction and specific primers for nopP2 as detailed in Table S6. Dilutions of plasmidic DNA containing cloned nopP2 gene sequence was used to generate standard curves in quantities ranging from 1 × 10² to 1 × 10⁷. Expression data were analyzed from three biological replicates across two independent experiments.

Identification of NopP2 interacting target proteins

The interacting partners or target proteins of NopP2 were identified using an *in vitro* pull-down assay. This assay used purified NopP2-His as bait and total root proteins from *V. radiata* cv. KPS1 as a prey.

Purified NopP2 tagged with 6×His were overproduced in *E. coli* BL21 (DE3) carrying NopP2-6×His-pET-19b. For the construction of NopP2-6×His-pET-19b, the full length of NopP2 (SPP98457.1) with the 6×His tagging at the C-terminus was amplified from the ORS3257 genome using specific primers listed in Table S6. The fragment was inserted into the pET-19b vector at *Ncol/Xbal* sites. For NopP2 expression and purification, *E. coli* BL21 (DE3) harboring NopP2-6×His-pET-19b was grown in LB supplemented with 100 μg/mL ampicillin on shaker (250 rpm) at 37°C for 18 h. The expression was induced by adding 1 mM IPTG at 30°C for 3 h. The purification was performed by Ni-NTA agarose beads (Qiagen), which were then exchanged with Tris-NaCl buffer using an Amicon Ultra centrifugal filter (Merck Millipore) before performing an *in vitro* pull-down assay. Finally, purified NopP2-6×His protein was observed in 12% SDS-PAGE and its concentration was measured using DC protein assay kits (Bio-Rad, USA) before use.

For the total plant proteins used in this experiment, we included proteins from *Vigna radiata* cv. KPS1 roots, both with and without bacterial infection, to ensure that we did not exclude any targets from either inducible or non-inducible proteins. Roots from 5-day-old plants inoculated with 1 mL of ORS3257 culture (OD600 = 1) were collected at 1 and 2 days post-inoculation (dpi) for protein extraction. The combined proteins extracted from these time points were designated as Root (+3257). In contrast, roots from non-inoculated plants were collected on the same days for protein extraction, and the proteins from these non-inoculated roots were designated as Root (NI). Total proteins from each condition were isolated from five replicate plants.

For protein extraction, three grams of fresh roots were ground in liquid nitrogen and suspended in an extraction buffer: 50 mM Tris-HCl (pH 8.0), 3 mM PMSF, 1% (v/v) 2-mercaptoethanol, 0.2% (v/v) Triton X-100, 10% (v/v) sucrose, and 10 mM ascorbic acid at a 1:5 tissue/buffer ratio. After centrifugation at $10,000 \times g$ for 30 min at 4° C, the supernatant without plant debris was transferred into a new tube and mixed with 30 mM DTT and one volume of Tris-HCl saturated phenol (pH 7.4). Then, the phenol phase was collected after centrifugation at $10,000 \times g$ for 30 min at 4° C and mixed with $400 \,\mu$ L 1 M DTT, $600 \,\mu$ L 4 M ammonium acetate, and 20 mL of methanol to precipitate proteins at 20° C overnight. The precipitated protein was collected by centrifugation ($10,000 \times g$ at 4° C for 1 h), and the pellet was washed with 70% (v/v) ethanol (cold). The pellet was well-dried and suspended with Tris-NaCl buffer. Finally, total root protein was observed in 12% SDS-PAGE, and its concentration was measured using the Bradford protein assay before use.

For the *in vitro* pull-down assay, $100 \,\mu$ l Ni-NTA agarose beads were used to purify NopP2-6×His ($10 \,\mu$ g). After washing, total proteins from Root (NI) or Root (+3257) ($400 \,\mu$ g in total) were loaded into columns and incubated at 4°C overnight. The column was washed with $500 \,\mu$ L washed buffer ($20 \,m$ M Tris-HCl (pH 7.4), $150 \,m$ M NaCl, $20 \,m$ M imidazole) 10 times. The trapped proteins in the column were eluted using elution buffer ($20 \,m$ M Tris-HCl (pH 7.4), $150 \,m$ M NaCl, $500 \,m$ M imidazole). The pull-down assay control was performed using a single incubation of total root proteins and NopP2-6×His. The eluted proteins from all treatments were observed using $12\% \,SDS$ -PAGE after staining.

MALDI-TOF MS/MS analysis

The selected bands were excised from the gel and subsequently subjected to trypsin digestion, which was performed using a MALDI-TOF MS/MS spectrometer (AB SCIEX 5800, SCIEX) and the MS-Fit ProteinProspector software (http://prospector.ucsf.edu/). MS/MS analysis was also performed using AB SCIEX 5800 and ProteinPilot Software (SCIEX). The protein database of *V. radiata* var. *radiata* (mung bean) was extracted from NCBI (Ref Seg assembly accession: GCF_000741045.1).

Confirmation of protein-protein interaction In vitro *pull-down assay*

Protein-protein interaction between NopP2 and 4 interacting partners was confirmed using an *in vitro* pull-down assay. This assay used purified NopP2-GST as the bait, whereas purified enolase (XP_014496230.1), glyceraldehyde-3-phosphate dehydrogenase (GAPDH; XP_014494377.1), monodehydroascorbate reductase (MDHAR; XP_014514196.1), serine hydroxymethyltransferase (SHMT; XP_014521732.1) and aspartate aminotransferase (AST; XP_014499632.1) tagged with 6×His were used as prey.

The purified NopP2-GST was overexpressed in *E. coli* BL21 (DE3) carrying NopP2-GST-pGEX-4T3. Construction was conducted as described in Table S6. NopP2-GST overexpression was performed at 25°C for 4 h with 1 mM IPTG induction. The soluble proteins were purified using glutathione beads 4FF (Bio Basic Asia Pacific, Singapore).

To produce purified four interacting proteins, all the recombinant plasmids of enolase, GAPDH, MDHAR, SHMT and AST with the tagging with 6×His were constructed into a pET-22b vector at the appropriate sites after amplifying the target fragments from the cDNA of *V. radiata* cv. KPS1 (described in Table S6). The overexpression of all proteins was performed under the same conditions as in NopP2-GST. The purification was performed using a Ni-NTA purification system, as previously mentioned. The purified NopP2-GST and all purified interacting proteins were observed using 12% SDS-PAGE and the target using Western blot analysis.

For the *in vitro* pull-down assay, 10 µg purified NopP2-GST was bound with glutathione beads before loading the purified proteins (30 µg of enolase-His, GAPDH-His, MDHAR-His, SHMT-His or AST-His). After the washing step, the total proteins in the column were



eluted with GST elution buffer (50 mM Tris-HCl, 50 mM glutathione (GSH), pH 8.0). A single incubation of each protein served as the control. The eluted proteins from all treatments were observed using 12% SDS-PAGE and detected using Western blot analysis.

ELISA assay

According to Eble⁴³ with some modifications, the Immuno 96 microWellTM plate (Nunc, Denmark) was immobilized with 10 μ g of recombinant His-tagged proteins at 4°C overnight and stabilized each well with 100 μ l stabilizer (5% sucrose, 0.3% BSA, and 50 mM NaHCO₃) for 45 min. The plate was washed twice with PBS and blocked with PBS containing bovine serum albumin (0.5% BSA in 1 x PBS) for 1 h at room temperature. The wells were washed twice with PBS after the removal of the blocking reagent. Then, 5 μ M of purified NopP2-GST and GST (control protein) were added to each well. After incubation for 1 h, remove unbound proteins and wash each well with four times PBST and two times PBS. After that, the protein with 100 μ L of 4% paraformaldehyde was incubated at room temperature for 45 min. The fixing solution was inactivated by adding an equal volume (100 μ L) of 20 mM Tris (pH 7.4) and 150 mM NaCl three times. Recombinant proteins conjugated with GST were detected using mouse anti-GST (1:5000) as the primary antibody, followed by Goat Anti-mouse Mouse (1:5000) as the secondary antibody. The color of the reaction was determined using ABTS reagent (Wako, Japan). The reaction was quantified by measuring the absorbance at 405 nm. The absorbance versus the concentration of the interacting protein was used to generate a binding curve. The apparent dissociation constant (Kd) was determined by nonlinear regression analysis.

Western blot analysis

For Western blot analysis, the recombinant proteins were blotted onto nitrocellulose membranes (Bio-Rad, USA) from the SDS polyacrylamide gel using a membrane transfer machine. The membrane was blocked with PBS containing skim milk (5% MPBS) for 1 h, followed by washing with PBS twice. Then, mouse anti-GST (Abbkine, USA) or/and mouse anti-HIS (Abbkine, USA) were used to detect the GST/HIS tag. The membrane was incubated with primary antibody at a dilution of 1:5000 in PBS for 1 h, followed by three wash steps with PBST and two times PBS. Subsequently, goat anti-mouse conjugated HRP (Abbkine, USA) diluted 1:5000 in PBS was added, and the membrane was incubated for 1 h before development. The Amersham ECL Western Blotting Detection Reagent (Cytiva, USA) was applied to the membrane according to the manufacturer's protocol for chemiluminescent signal detection.

Subcellular localization in planta

NopP2 and all interacting proteins (enolase, GAPDH, MDHAR and SHMT) were overexpressed in mung bean root using the *Agrobacterium* transformation method. NopP2 was fused with GFP in the pCAMBAl1302 vector, while interacting proteins, including enolase, GAPDH, MDHAR, and SHMT, were fused with mCherry in the modified pCAMBIA1302 vector. All of the recombinant proteins were controlled under the CaMV35S promotor. The construction of all recombinant plasmids was performed by PCR amplification using specific primers, as described in Table S6. All recombinant plasmids were transferred into *A. rhizogenes* strain K599 via electroporation (20 kV, $50 \,\mu$ F capacitance, 200 Ohm resistance, and 0.2-cm cuvette). The transferred strains were selected from LB containing kanamycin ($50 \,\mu$ g/mL).

To generate transgenic roots, V. radiata cv. KPS1 was germinated in sterilized vermiculite for 3 days. Two-day-old colonies of A. rhizogenes strain K599 harboring each of recombinant plasmid (NopP2-GFP, enolase-mCherry, GAPDH-mCherry, MDHARmCherry and SHMT-mCherry) was directly used to inject into the stem under the hypocotyl of healthy and uniform plants via needle punching. To determine the co-localization between NopP2 and each interacting protein, mixed cultures of Agrobacterium strains (NopP2:enolase, NopP2:GAPDH, NopP2:MDHAR and NopP2:SHMT) were injected into plants by needle punching as previously described. Plants were grown under controlled environmental conditions, as mentioned above. The transgenic roots at the injection site were selected under a fluorescent stereomicroscope before performing 40 µm thick sections using a VT1000S vibratome (Leica Nanterre, France). To enhance the GFP signal from NopP2-GFP in root tissue, sectioned roots were immunolocalized using an antibody for GFP detection. Briefly, tissues were fixed in 4% formaldehyde in MTSB buffer (50 mM PIPES, 5 mM EGTA, 5 mM MgSO₄·7H₂O, pH 7.0) supplemented with 0.1 % Triton X-100 at room temperature for 1 h. The tissues were washed with MTSB buffer four times before cell wall digestion with digestion solution (2% (v/v) Driselase in MTSB buffer) at room temperature for 1 h. After washing (4 times), it was blocked with 3% BSA (in MTSB buffer) for 2 h at room temperature. Mouse anti-GFP (Abbkine, USA) (1:2000 diluted in 3% BSA) was used to detect NopP2-GFP. After overnight incubation at 4°C, tissues were washed six times and then incubated with a secondary antibody (goat anti-mouse conjugated with Alexa Fluor 488, Thermo ScientificTM, USA) at 37°C for 2h. After washing, tissues were stained with 2 μg 4',6-diamidino-2-phenylindole (DAPI, Thermo ScientificTM, USA) for 15 min to visualize nuclei. The tissues were observed using an Olympus Fluoview FV1000 confocal laser scanning microscope.

To confirm the subcellular localization of NopP2 and its four interacting proteins, Agroinfiltration was performed on *Nicotiana benthamiana* leaves. All recombinant plasmids were introduced into *A. tumefaciens* strain AGL1 via electroporation. The cell pellets from two-day-old cultures were collected by centrifugation (6,000 rpm, 5 min) and resuspended in MMA (10 mM MgCl2, 10 mM MES [pH 5.6], 150 μ M acetosyringone) to a final optical density at 600 nm (OD₆₀₀) of 0.04. Using the syringe, 100 μ L of cell suspension was infiltrated per spot on the underside of a fully expanded leaf. Infected plants were maintained on shelves under controlled environmental conditions at 22°C with a 16 h/8 h. light/dark photoperiod. For co-localization studies between NopP2 and each interacting protein, the mixed cultures (1:1) of *Agrobacterium* strains (NopP2:enolase, NopP2:GAPDH, NopP2:MDHAR and NopP2:SHMT) were infiltrated as described above. To visualize nuclei, the epidermis was stained with DAPI (2 μ g/mL) for 15 min and the stained leaves were washed twice. Subcellular localization and co-localization were observed using Nikon AX/AXR confocal microscope (Nikon Instruments Inc.) at 4 days after infiltration.





Transcriptome analysis and gRT-PCR

Transcriptome analysis of V. radiata cv. KPS1 roots in response to nodulation by B. vignae ORS3257 was conducted using total root RNA collected at 2 and 3 days post-inoculation (dpi). Briefly, sterilized seeds were germinated overnight before being transplanted into sterilized vermiculite in Leonard's jars, as previously described. Five-day-old plants were then inoculated with ORS3257 and Ω nopP2 strains at an OD₆₀₀ of 1 (approximately 10⁹ cells/mL). At harvest (2 and 3 dpi), roots were collected for total RNA extraction using the FavorPrep Plant Total RNA Purification Mini Kit (Favorgen) following the manufacturer's instructions. RNA quality was assessed using an Agilent 2100/2200 Bioanalyzer (Agilent Technologies), NanoDrop (Thermo Scientific), and 1% agarose gel electrophoresis. Next-generation sequencing (NGS) library preparation was then performed. Transcriptome analysis included non-inoculated controls, ORS3257-inoculated roots, and Ω nopP2-inoculated roots, combining RNA samples from 2 and 3 dpi after each treatment. Each library was sequenced using an Illumina HiSeg platform (paired-end 150 bp reads) by Azenta Life Sciences.

For relative gene expression analysis using qRT-PCR, total RNA was isolated from KPS1 roots inoculated with ORS3257 and ΩnopP2 strains at 1, 2, 3, and 5 days post-inoculation (dpi), following the previously described STAR Methods. Additionally, total RNA from non-inoculated roots at the same time points was also analyzed. One microgram of total RNA was used for cDNA synthesis with the iScriptTM cDNA Synthesis Kit (Bio-Rad) according to the manufacturer's instructions. Quantitative real-time PCR (qRT-PCR) was performed using Luna® Universal qPCR Master Mix (NEB, USA) with 5 ng of cDNA per reaction and the specific primers listed in Table S6. Relative gene expression was determined using the comparative Ct ($2^{-\Delta\Delta CT}$) method, with Actin as the reference gene (Table S6). 44 Expression data were analyzed in triplicate biological experiments in two independent experiments.

MDHAR activity and hydrogen peroxide (H₂O₂) accumulation in roots

MDHAR activity was measured in non-inoculated controls, ORS3257-inoculated roots, and Ω nopP2-inoculated roots at 5 dpi using spectrophotometry by monitoring the decrease in absorbance at 340 nm due to NADH oxidation. A hundred milligrams of roots were homogenized in liquid nitrogen, and added 1 ml of extraction buffer (50 mM potassium phosphate buffer, pH 7.0, 10% PVP, 0.25% Triton X-100, 1mM PMSF and 1mM ascorbate). The reaction mixture contained 50 mM HEPES buffer (pH 7.6), 0.25 mM NADH, 2.5 mM ascorbate, 0.5 units of ascorbate oxidase, and 10 μL of the extracted samples. The reaction was initiated by adding the enzyme extract to the mixture, and the rate of NADH oxidation was recorded after 20 min at 25°C. One unit of MDHAR activity was defined as the amount of enzyme that oxidizes 1 nmol of NADH per minute. The activity was calculated using an extinction coefficient of 6.22 mM⁻¹ cm⁻¹ for NADH and demonstrated in nmol min⁻¹ mg⁻¹ protein.

The accumulation of H₂O₂ in roots was detected by staining with DAB (3,3'-diaminobenzidine tetrachloride) following the protocol described by Libik-Konieczny et al. 45

Phylogenetic tree construction and protein alignment

The phylogenetic trees of NopP proteins from various rhizobial strains were constructed using the Neighbor-Joining method in the Molecular Evolutionary Genetics Analysis (MEGA11) software. Bootstrap values, derived from maximum-likelihood analysis, are indicated at the nodes and branches of the trees. Amino acid alignment was performed using the Multalin program (http://multalin. toulouse.inra.fr/multalin/cgi-bin/multalin.pl).46

QUANTIFICATION AND STATISTICAL ANALYSIS

Quantification for RNA-seq

The reference genome was V. radiata var. radiata (mung bean) (NCBI ID: GCF_000741045.1). Differentially expressed genes (DEGs) were identified using a p-value threshold of 0.05 and a fold-change cutoff of log₂FC > 1. Gene Ontology (GO) enrichment analysis was then performed to categorize up-regulated (p-value < 0.05, log₂FC > 1) and downregulated (p-value < 0.05, log₂FC < -1) genes, comparing their functions with those observed ORS3257-inoculated roots, and Ω nopP2-inoculated roots.

Statistical analysis

Mean values and standard division (SD) were analyzed using SPSS software (SPSS version 26.0 Windows; SPSS Inc., Chicago, IL). Mean comparisons were conducted using two-way analysis of variance (ANOVA) and multiple comparisons, with significance levels set at p-value < 0.05 (*), p-value < 0.001 (***) and p-value < 0.0001 (***), while p-value > 0.05 indicated as not significantly different (NS).